

# Spin-Orbit Physics Giving Rise to Novel Phases in Correlated Systems; Iridates and Related Materials

Jeffrey G. Rau

*Department of Physics and Astronomy, University of Waterloo, Ontario, N2L 3G1, Canada*

Eric Kin-Ho Lee

*Department of Physics and Center for Quantum Materials,  
University of Toronto, Toronto, Ontario, M5S 1A7, Canada*

Hae-Young Kee\*

*Department of Physics and Center for Quantum Materials,  
University of Toronto, Toronto, Ontario, M5S 1A7, Canada and  
Canadian Institute for Advanced Research/Quantum  
Materials Program, Toronto, Ontario, MSG 1Z8, Canada*

(Dated: July 24, 2015)

Recently, the effects of spin-orbit coupling (SOC) in correlated materials have become one of the most actively studied subjects in condensed matter physics, as correlations and SOC together can lead to the discovery of new phases. Among candidate materials, iridium oxides (iridates) have been an excellent playground to uncover such novel phenomena. In this review, we discuss recent progress in iridates and related materials, focusing on the basic concepts, relevant microscopic Hamiltonians, and unusual properties of iridates in perovskite- and honeycomb-based structures. Perspectives on SOC and correlation physics beyond iridates are also discussed.

**Keywords:** Superconductivity, Magnetism, Topological, Spin liquid, Perovskite iridates, Honeycomb iridates, Transition metal

## CONTENTS

|   |    |
|---|----|
| I. Introduction   | 2  |
| II. Background  | 3  |
| III. Magnetism, topological phases and superconductivity in perovskite iridates | 5  |
| A. Magnetism  | 6  |
| B. Corner shared octahedra with strong spin-orbit coupling                      | 7  |
| C. Distortions and octahedral rotations   | 8  |
| D. Topological phases   | 10 |
| E. Superconductivity  | 12 |
| IV. Spin liquids and unconventional magnetic orders in honeycomb iridates       | 15 |
| A. Spin-orbit Mott insulators with edge-shared octahedra                        | 15 |
| B. Distortions  | 16 |
| C. Kitaev physics in two dimensions   | 17 |
| 1. Experimental review  | 18 |
| 2. Theory   | 19 |
| 3. $\alpha$ -RuCl <sub>3</sub>  | 21 |
| D. Kitaev physics in three dimensions   | 22 |
| 1. Experimental review  | 23 |
| 2. Theory   | 23 |
| V. Outlook  | 25 |
| Acknowledgments   | 28 |
| References  | 28 |

## I. INTRODUCTION

Spin-orbit coupling (SOC) is a relativistic effect that links the orbital and spin angular momenta of an electron. Though suppressed by the fine structure constant, the electric fields near the nuclei of atoms with a large number of protons can render this interaction significant. The natural place to find significant SOC is thus in atoms with high atomic numbers, moving down the rows of the periodic table into the heavier elements.

The effects of SOC in materials with such heavy atoms have been studied intensively in the context of semi-conductors. In these weakly correlated materials, SOC entangles the crystal momentum and spin of the electron, locking the kinetic and internal degrees of freedom together. This leads to a number of intriguing phenomena, particularly in transport; examples include the

anomalous Hall effect (AHE) and the control of spin currents being applied in the field of spintronics. More recently it has been found that SOC plays an essential role in the fast growing field of topological insulators (TI) and metals. Many, if not all, of the experimental examples of such topological phases have been found in these types of heavy semi-conductors.

While the effects of SOC in weakly correlated materials described above has been thoroughly considered, its importance in more strongly correlated transition metal materials remains less developed. There are several energy scales to consider in such materials: the atomic interactions (schematically) on-site Hubbard interaction  $U$ , Hund's coupling  $J_H$ , the SOC  $\lambda$ , the crystal field  $\Delta$  and the electron kinetic energy described by hopping integral  $t$ . Much theoretical and experimental effort has been brought to bear on  $3d$  transition metals such as high temperature cuprates, manganites, and vanadium oxides. In these compounds the atomic interactions, crystal field and kinetic terms can generally compete, though the SOC remains small. In heavy transition metals such as those with  $5d$  and even  $4d$  electrons SOC is significant as well, and so all of these energy scales can be comparable. As one moves through the different heavy transition metal materials, small changes in these details can tip the scales, revealing a surprisingly rich family of behaviours. This can be contrasted with  $4f$  or  $5f$  electrons in the lanthanides or actinides, where the electron interactions are dominant, followed by the SOC and then the crystal fields.

While intensive studies have recently been undertaken, we are still far from complete understanding on the combined effects of SOC and electronic correlation. Material examples of  $4d$  and  $5d$  systems can be found for a variety of two- and three-dimensional lattices with varying degrees of frustration, covering the range from weakly to strongly correlated. An excellent overview of this physics is provided in a recent review<sup>1</sup>, with a focus on examples from the pyrochlore iridates and the  $5d$  double-perovskite magnets. In this review we will focus on magnetism, topological phases and superconductivity induced by the competition between strong SOC and electronic correlation. We illustrate these concepts with examples drawn from the perovskite and honeycomb iridium oxides. After a basic introduction to the relevant models in Sec. II, we begin with perovskite iridates in Sec. III. Drawing analogies to the related cuprates and ruthenates, we discuss proposals for realizing topological and superconducting phases in the materials. In Sec. IV we tackle the burgeoning field of Kitaev magnetism. In particular, we offer a summary of the current status of two- and three-dimensional honeycomb iridates. Concluding remarks and outlook are provided in Sec. V.

## II. BACKGROUND

The building blocks of our discussion are the atomic states of the partially filled  $4d$ - or  $5d$  ions. In solids of interest, these states are split by a predominantly octahedral crystal field potential into a  $t_{2g}$  triplet and  $e_g$  doublet, as shown in Fig. 1. The energy gap to the  $e_g$  doublet is large, so these states can be safely ignored when we consider electron filling less than six. We are primarily interested in the  $d^5$  configuration, which can be regarded as single hole in one of the  $t_{2g}$  states.

When projected into this manifold, the angular momentum of the the  $d$  electrons is mapped to a set of effective  $l = 1$  angular momentum operators,  $-\mathbf{L}$ . The large SOC then acts within the  $t_{2g}$  manifold as  $-\lambda \mathbf{L} \cdot \mathbf{S}$  where  $\mathbf{L}$  is an effective  $l = 1$  angular momentum and  $\mathbf{S}$  is the spin. Using the rules of addition of angular momenta we see that SOC splits the  $t_{2g}$  multiplet into an effective  $j = 1/2$  doublet and effective  $j = 3/2$  quartet as show in Fig. 1. The  $j = 3/2$  states are lower in energy and separated from the  $j = 1/2$  states by a gap of  $3\lambda/2$ . Written in terms of the  $t_{2g}$  states one has

$$\left| \frac{1}{2}, \pm \frac{1}{2} \right\rangle = \sqrt{\frac{1}{3}} (|yz, \mp\rangle \pm i |xz, \mp\rangle \pm |xy, \pm\rangle), \quad (1a)$$

$$\left| \frac{3}{2}, \pm \frac{3}{2} \right\rangle = \sqrt{\frac{1}{2}} (|yz, \pm\rangle \pm i |xz, \pm\rangle), \quad (1b)$$

$$\left| \frac{3}{2}, \pm \frac{1}{2} \right\rangle = \sqrt{\frac{1}{6}} (|yz, \mp\rangle \pm i |xz, \mp\rangle - 2 |xy, \pm\rangle), \quad (1c)$$

where  $|yz, \pm\rangle, |xz, \pm\rangle, |xy, \pm\rangle$  are the  $t_{2g}$  states and spin up and down correspond to  $\pm$ . The important role played by SOC can be seen in the entanglement of the spin and orbital degrees of freedom in these wave-functions, as illustrated in Fig. 1. The states of this  $j = 1/2$  doublet and its pseudo-spin operators  $\mathbf{J}$  will be a common thread in our discussion of the family of iridium oxides and ruthenium materials. While strongly spin-orbit entangled, it remains *isotropic*, with a  $g$ -factor of  $-2$ . Explicitly, the magnetic moment operator  $\boldsymbol{\mu} = \mu_B (\mathbf{L} + 2\mathbf{S})$  becomes  $-2\mu_B \mathbf{J}$  when projected into the  $j = 1/2$  states. The anisotropy of these systems thus manifests predominantly in the *coupling* of  $j = 1/2$  moments<sup>2</sup>, not in the single-ion properties.

The interactions of  $j = 1/2$  electrons are determined by the atomic interactions of the free ion projected into the  $t_{2g}$  manifold and the kinetic terms, or hoppings of the  $t_{2g}$  electrons. Schematically we can write the general multi-orbital model

$$\sum_{ij} \sum_{\alpha\beta} \sum_{\sigma} t_{ij}^{\alpha\beta} (d_{i\alpha\sigma}^{\dagger} d_{j\beta\sigma} + \text{h.c.}) + \sum_i \left[ \left( \frac{U - 3J_H}{2} \right) (N_i - 5)^2 - 2J_H \mathbf{S}_i^2 - \frac{J_H}{2} \mathbf{L}_i^2 - \lambda \mathbf{L}_i \cdot \mathbf{S}_i \right], \quad (2)$$

where  $N_i$  is the total number operator,  $\mathbf{S}_i$  is the total spin operator and  $\mathbf{L}_i$  is the total pseudo-angular momentum operator at site  $\mathbf{r}_i$ . The  $d_{i\alpha\sigma}^{\dagger}$  operator creates a  $t_{2g}$  electron in orbital  $\alpha = yz, xz$  or  $xy$  with spin  $\sigma = \uparrow, \downarrow$  at site  $\mathbf{r}_i$  and  $t_{ij}^{\alpha\beta}$  are the tight-binding hopping parameters. The hopping amplitudes  $t_{ij}^{\alpha\beta}$  will have contributions coming from direct  $d$ - $d$  overlap, as well as from processes through the intermediate oxygen atoms. As these kinetic terms are strongly material dependent in both structure and scale, we save discussion of their details for the sections devoted to each specific class of material.

The local atomic interactions are more generic and can be expressed in terms of two parameters<sup>3</sup>: the Coulomb repulsion  $U$  and the Hund's coupling  $J_H$ . We have added a chemical potential to favour the  $N = 5$  state relevant for  $\text{Ir}^{4+}$  and  $\text{Ru}^{3+}$  and have fixed the inter-orbital repulsion  $U'$  to the free ion value  $U - 2J_H$ . Typically one expects  $U \sim 2 \text{ eV}$ <sup>4</sup>,  $J_H \sim 0.2 \text{ eV}$  and  $3\lambda/2 \sim 0.4 - 0.5 \text{ eV}$ <sup>5</sup> for an  $\text{Ir}^{4+}$  ion. On the other hand for a  $\text{Ru}^{3+}$  ion,  $U$  and  $J_H$  are stronger while atomic SOC is weaker

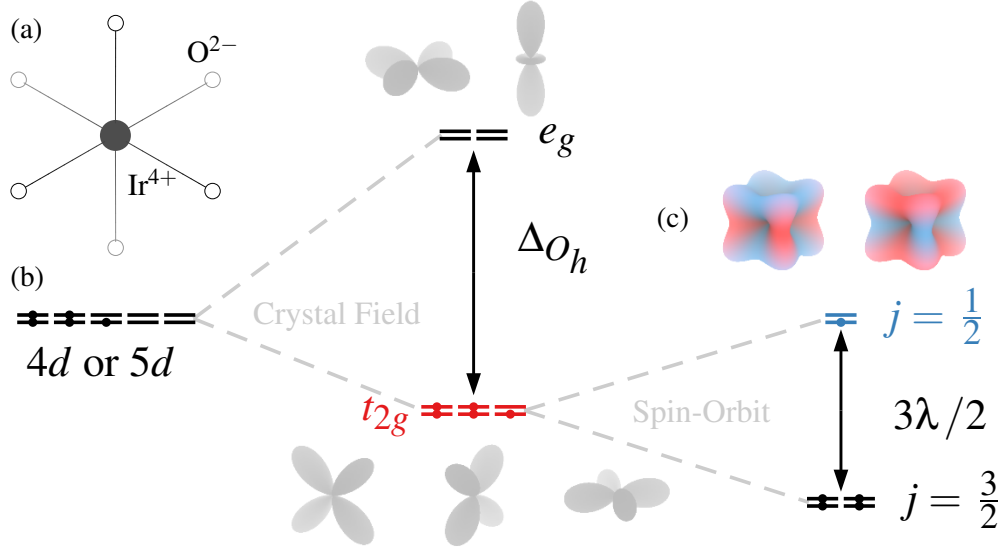


FIG. 1: (a) Octahedral geometry of transition metal site illustrated for an iridium oxide. (b) Splitting of the 4d or 5d levels by octahedral crystal fields  $\Delta_{O_h}$  and by SOC  $\lambda$  into  $j = 1/2$  and  $j = 3/2$  levels. (c) Illustration of the atomic  $j = 1/2$  wave-functions. The composition of the  $j = 1/2$  states with the spin- $\uparrow$  charge density is shown in red and the spin- $\downarrow$  charge density in blue.

than the Ir<sup>4+</sup> case. Due to screening effects in a solid, these parameters will be renormalized, and the free ion relation  $U' = U - 2J_H$  can be violated. Typically, one expects the Coulomb integral  $U$  to be more strongly screened than the Hund's coupling  $J_H$ <sup>3,4</sup>.

There are several limiting regimes where the physics of this model is particularly clear. In Sec. III we will consider the limit where the interactions between the  $j = 1/2$  and  $j = 3/2$  electrons can be neglected. This yields an effective single-band Hubbard model for the  $j = 1/2$  electrons. With sufficiently weak correlations, this approximation can be useful as a starting point for itinerant single band  $j = 1/2$  systems. In the strongly correlated regime, the  $j = 1/2$  electrons localize and one is left with a pseudo-spin model. By projecting into only the  $j = 1/2$  states one loses the  $j = 3/2$  excited states and the effects of Hund's coupling. As we will see in Sec. IV, for the honeycomb iridates, this leading term may *cancel*, so the contribution of the virtual processes that go through  $j = 3/2$  states become the largest interactions.

### III. MAGNETISM, TOPOLOGICAL PHASES AND SUPERCONDUCTIVITY IN PEROVSKITE IRIDATES

Historically, the field began with the study of Sr<sub>2</sub>IrO<sub>4</sub> and Sr<sub>2</sub>RuO<sub>4</sub> as isostructural analogues of La<sub>2</sub>CuO<sub>4</sub>, the parent compound of the cuprate superconductors. While Sr<sub>2</sub>IrO<sub>4</sub> was first synthesized in 1957<sup>11</sup>, early work focused mainly on chemical aspects, with variety of ternary and quaternary oxides of iridium and ruthenium reported in the following decades.<sup>12</sup> More serious interest in Sr<sub>2</sub>IrO<sub>4</sub> was piqued when superconductivity was discovered in Sr<sub>2</sub>RuO<sub>4</sub><sup>13</sup>, but an insu-

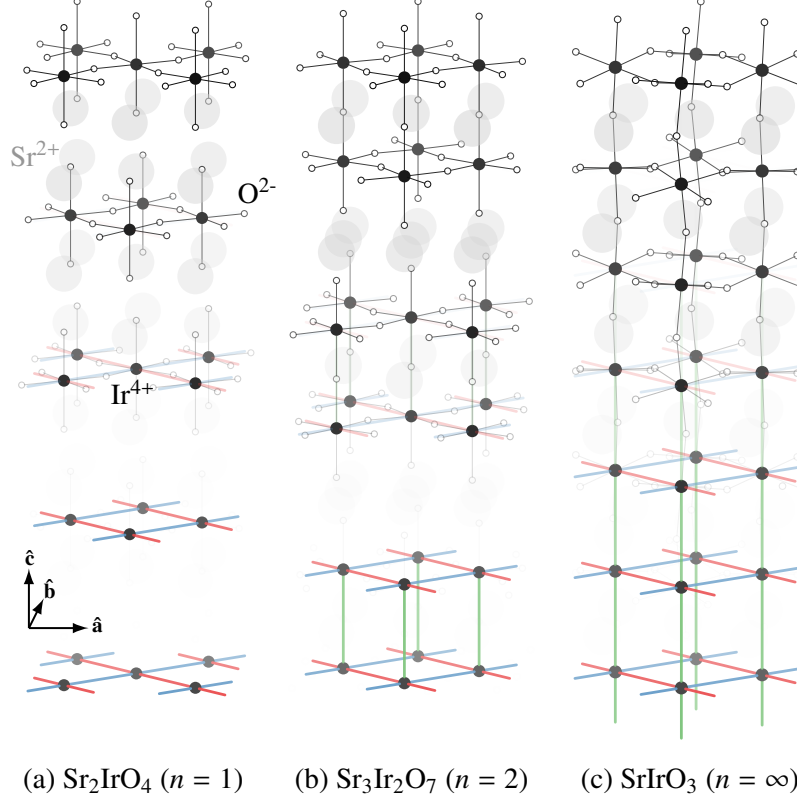


FIG. 2: Crystal structures of the perovskite iridates from the Ruddlesden-Popper series  $\text{Sr}_{n+1}\text{Ir}_n\text{O}_{3n+1}$ . These include the quasi-two dimensional (a) single-layer  $\text{Sr}_2\text{IrO}_4$ <sup>6,7</sup>, and (b) bilayer  $\text{Sr}_3\text{Ir}_2\text{O}_7$ <sup>8</sup> and the three dimensional limit (c) orthorhombic  $\text{SrIrO}_3$ <sup>9,10</sup>.

lating state with small ferromagnetic moment was found instead<sup>6,14</sup>. Interest was renewed by the discovery that the interplay between SOC and electronic correlations were driving the physics in this material<sup>5,15</sup>.

In this section, our primary focus will be on magnetism in  $\text{Sr}_2\text{IrO}_4$  and  $\text{Sr}_3\text{Ir}_2\text{O}_7$  and the possible realization of novel topological phases and superconductivity. We start with a review of the experimental and theoretical progress in understanding perovskite iridates such as the Ruddlesden-Popper series of  $\text{Sr}_{n+1}\text{Ir}_n\text{O}_{3n+1}$  through a discussion of the common building block of corner-shared octahedra in both the itinerant and localized limits. Next, we discuss some candidate topological phases built from iridium oxide heterostructures. Finally, we discuss the effects of charge doping, with an eye toward the possibility of superconductivity in  $\text{Sr}_2\text{IrO}_4$ .

### A. Magnetism

In the single and bilayer perovskites  $\text{Sr}_2\text{IrO}_4$  and  $\text{Sr}_3\text{Ir}_2\text{O}_7$ <sup>16</sup> evidence from the optical gap<sup>17</sup> to the magnetic ordering transition<sup>14,18–20</sup> have indicated that both are Mott insulators, though  $\text{Sr}_3\text{Ir}_2\text{O}_7$  being substantially weaker than  $\text{Sr}_2\text{IrO}_4$ . The modest on-site Hubbard interaction  $U$

proves sufficient to localize the electrons due to the narrow, spin-orbit coupled  $j = 1/2$  bands. In  $\text{Sr}_2\text{IrO}_4$  the magnetic ordering is an in-plane, canted antiferromagnet<sup>15,21</sup> following the staggered rotation of the oxygen octahedra, as illustrated in Fig. 3a. Though the net ferromagnetic moment of this state was observed in early studies<sup>6,7,14</sup>, the crucial role played by strong SOC was only understood fairly recently<sup>22</sup>. The moment directions in  $\text{Sr}_3\text{Ir}_2\text{O}_7$  are very different, forming a collinear arrangement perpendicular to the iridium planes<sup>20</sup> as shown in Fig. 3c.

The bulk trilayer and higher compounds ( $n \geq 3$ ) are unstable under ambient pressure<sup>23</sup>, including the three-dimensional limit  $\text{SrIrO}_3$  which takes a post-perovskite structure<sup>9</sup>. An orthorhombic perovskite  $\text{SrIrO}_3$  can be stabilized via the application of pressure; this is a semi-metal and shows no evidence of magnetic ordering<sup>10,17</sup>. One can then posit<sup>17</sup> a metal-insulator transition (MIT) exists as a function of layer count near  $n_c \sim 3$ , placing  $\text{Sr}_2\text{IrO}_4$  ( $n = 1$ ) and  $\text{Sr}_3\text{Ir}_2\text{O}_7$  ( $n = 2$ ) on the insulating side and orthorhombic  $\text{SrIrO}_3$  ( $n = \infty$ ) on the metallic side. Due to the proximity to this putative MIT there has been some debate on the applicability of the strongly coupled Mott picture as compared to a more weakly coupled Slater picture<sup>24–26</sup>. Since the weak and strong-coupling regimes give the same magnetic orderings,<sup>26</sup> this distinction may be somewhat academic at low temperature. Near the transition the Mott and Slater regimes could be distinguishable through the behaviour of the charge gap.

Key questions to address in these compounds concern both the magnetic ordering and the MIT. In particular, we wish to understand what sets the direction of the ordered moments in  $\text{Sr}_2\text{IrO}_4$ , and  $\text{Sr}_3\text{Ir}_2\text{O}_7$ . Beyond this we would like to establish a framework understanding both the itinerant and localized limits of this family of compounds. This will provide useful guidance for our discussion of *engineered phases* constructed from the same basic building block in Sec. III D.

## B. Corner shared octahedra with strong spin-orbit coupling

The perovskite iridates are built from corner-shared octahedra as shown for  $\text{Sr}_2\text{IrO}_4$ ,  $\text{Sr}_3\text{Ir}_2\text{O}_7$  and orthorhombic  $\text{SrIrO}_3$  in Fig. 2. The observed MIT<sup>17</sup> as a function of layer count makes it necessary to discuss both the weak and strong correlation limits. Here, we present a brief account of the  $j = 1/2$  spin models at strong coupling, as well as the tight-binding models at weak coupling that is applicable to all networks of corner-shared octahedra. While the real materials have structural distortions, we begin with the idealized, undistorted limit.

One simple approach to attacking the model in Eq. (2) is to assume the  $j = 1/2$  and  $j = 3/2$  bands to be well separated, neglecting the inter-band interactions. This projects the multi-orbital problem of Eq. (2) into a single-band model of  $j = 1/2$  electrons with an effective hopping and Hubbard interaction

$$\sum_{ij} \sum_{\alpha=\pm} t_{ij} (c_{i\alpha}^\dagger c_{j\alpha} + c_{j\alpha}^\dagger c_{i\alpha}) + U_{\text{eff}} \sum_i n_{i+} n_{i-}, \quad (3)$$

where  $c_{i\pm}^\dagger$  creates a  $j_z = \pm 1/2$  electron at site  $\mathbf{r}_i$  and  $U_{\text{eff}} \sim (U + 2U')/3$ . Inversion and time-reversal symmetry forbid pseudo-spin dependent hoppings. This type of itinerant model is a useful starting



point to describe the more three-dimensional compounds, such as those based on  $\text{SrIrO}_3$ . Due to the increased dimensionality, the bandwidth of the  $j = 1/2$  states is larger than the quasi-two-dimensional compounds and becomes comparable to the effective Coulomb  $U_{\text{eff}}$ .

The magnetic ordering in these models is most easily approached from the strong Mott limit where  $U_{\text{eff}} \gg t$ . Assuming the nearest-neighbour hoppings are dominant, this yields an antiferromagnetic Heisenberg model with an effective  $\text{SU}(2)$  pseudo-spin rotation symmetry<sup>22</sup>

$$\frac{4t^2}{U_{\text{eff}}} \sum_{\langle ij \rangle} \mathbf{J}_i \cdot \mathbf{J}_j, \quad (4)$$

where  $\mathbf{J}_i$  is the  $j = 1/2$  pseudo-spin at site  $\mathbf{r}_i$  and  $t$  is the nearest-neighbour  $j = 1/2$  hopping. Going back to Eq. (2) and including the  $j = 3/2$  excited states or the Hund's coupling spoils this accidental symmetry and generates all symmetry allowed terms. For an ideal corner-shared,  $180^\circ$  bond these include a four-fold rotation about the bond direction, and several reflections. The symmetry allowed terms include a Heisenberg exchange  $J$  and a compass-like, pseudo-dipolar coupling  $K$ <sup>22</sup>

$$\sum_{\langle ij \rangle} [J \mathbf{J}_i \cdot \mathbf{J}_j + K (\hat{\mathbf{r}}_{ij} \cdot \mathbf{J}_i)(\hat{\mathbf{r}}_{ij} \cdot \mathbf{J}_j)], \quad (5)$$

where  $\mathbf{r}_{ij} \equiv \mathbf{r}_j - \mathbf{r}_i$  is the bond direction. In concrete models<sup>22</sup> one finds  $K/J \propto J_H/U$ , so we expect the Heisenberg term to dominant, with only a small pseudo-dipolar coupling  $K \ll J$ .

The structure of this simple model provides a partial answer to the experimental questions introduced in Sec. III A. Namely, the approximate  $\text{SU}(2)$  symmetry renders the final pinning of the magnetic moments sensitive to  $\text{SU}(2)$  breaking perturbations, such as the pseudo-dipolar coupling  $K$ . Due to this sensitivity, to understand the fate of these moments we must understand the complete set of structural distortions present in the perovskite iridates.

### C. Distortions and octahedral rotations

Two relevant types of distortions in the perovskite iridates are tetragonal distortion and octahedral rotations. The former arises in the layered compounds such as  $\text{Sr}_2\text{IrO}_4$  and  $\text{Sr}_3\text{Ir}_2\text{O}_7$ , while octahedral rotations are present in the entire Ruddlesden-Popper series. Due to the layered structure, the octahedra in  $\text{Sr}_2\text{IrO}_4$  and  $\text{Sr}_3\text{Ir}_2\text{O}_7$  are elongated along the inter-layer direction,  $[001]$ <sup>6–8,27</sup>. Such local distortions can be encapsulated in a residual crystal field potential that split the  $j = 3/2$  levels into two Kramers doublets which remain well separated from the higher-lying doublet for small distortion<sup>2</sup>. This highest lying doublet plays the role the  $j = 1/2$  does in the ideal case and defines our pseudo-spin. In their simplest form, these distortions manifest as a compression or elongation along some direction  $\hat{\mathbf{n}}$  of the octahedron, modeled as

$$V_{\hat{\mathbf{n}}} = \Delta (\hat{\mathbf{n}} \cdot \mathbf{L})^2, \quad (6)$$

where  $\mathbf{L}$  is the orbital angular momentum projected into the  $t_{2g}$  levels and  $\Delta > 0$  corresponds to compression and  $\Delta < 0$  to elongation. For tetragonal distortion  $\hat{\mathbf{n}}$  is along one of the cubic axes,



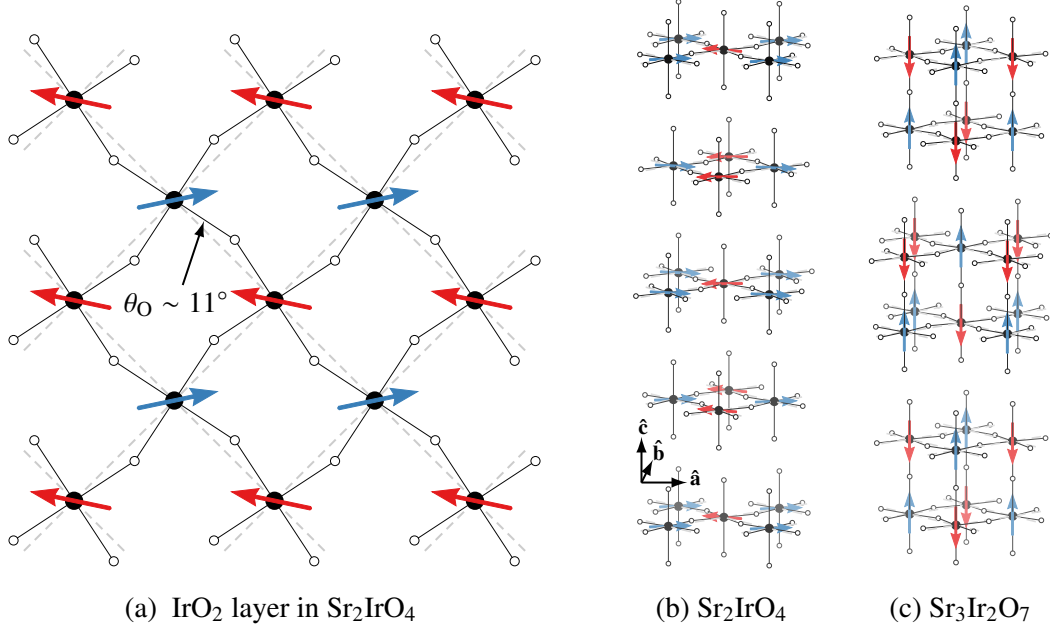


FIG. 3: Illustration of octahedral rotations and magnetic canted antiferromagnetic order in  $\text{Sr}_2\text{IrO}_4$ <sup>15,21</sup>. (a) The octahedral rotations and moment directions in a single  $\text{IrO}_2$  plane of  $\text{Sr}_2\text{IrO}_4$ . (b-c) Illustration of the stacking of planes and the ordering in (b)  $\text{Sr}_2\text{IrO}_4$ <sup>15,21</sup> and (c)  $\text{Sr}_3\text{Ir}_2\text{O}_7$ <sup>20</sup>.

$\hat{x}$ ,  $\hat{y}$  or  $\hat{z}$ . Including the SOC, the atomic energy levels can be straightforwardly found, with the highest lying doublet being a mixture of the  $j = 1/2$  and  $j = 3/2$  states as<sup>2</sup>

$$|\pm\rangle = \cos\theta \left| \frac{1}{2}, \pm\frac{1}{2} \right\rangle \pm \sin\theta \left| \frac{3}{2}, \pm\frac{1}{2} \right\rangle, \quad (7)$$

where the mixing angle is  $\tan(2\theta) = 4\sqrt{2}\Delta/(2\Delta + 9\lambda)$ . Including these distortions removes the effective four-fold rotation symmetry, allowing an additional Ising-like anisotropy  $\sim \Gamma_{zz}J_i^zJ_j^z$  on each bond in the plane perpendicular to the distortion<sup>22</sup>.

In addition, octahedral rotations are present and break some of the rotational and translational symmetry of the ideal lattice, enlarging the unit cell. In  $\text{Sr}_2\text{IrO}_4$  and  $\text{Sr}_3\text{Ir}_2\text{O}_7$  the octahedra are rotated about the  $[001]$  axis in a staggered fashion<sup>6-8</sup>, characterized by a deviation of the bond angle of  $\sim 11^\circ \equiv \theta_0$  from the ideal  $180^\circ$ , as illustrated in Fig. 3a. We leave the more involved octahedral tilting of orthorhombic  $\text{SrIrO}_3$  to the literature<sup>9,10</sup>. Such rotations lower the bond symmetry, breaking the inversion symmetry about the bond center and allow pseudo-spin dependent hoppings and Dzyaloshinskii-Moriya (DM) exchange<sup>22,28</sup>. Schematically, a tight-binding model for the  $j = 1/2$  electrons in a single  $\text{IrO}_2$  plane that includes such effects is

$$\sum_{\langle ij \rangle} \left[ -t \sum_{\alpha} (c_{i\alpha}^\dagger c_{j\alpha} + \text{h.c.}) + it_z \sum_{\alpha\alpha'} (-1)^i (c_{i\alpha}^\dagger \sigma_z c_{j\alpha'} + \text{h.c.}) \right], \quad (8)$$

where  $(-1)^i = \pm 1$  is a staggered sign, as illustrated in Fig. 3a and one expects  $t \sim \cos 2\theta_0$  and  $t_z \sim \sin 2\theta_0$ . The pseudo-spin dependent term  $t_z$  can be removed by rotating the pseudo-spin at

each site by an angle  $(-1)^i\phi$  about the  $\hat{z}$  axis, where  $\tan 2\phi = t_z/t^{28}$ . In these rotated axes the effective spin model is once again purely Heisenberg<sup>22</sup>, with  $J \sim 4(t^2 + t_z^2)/U_{\text{eff}}$ , without the DM or symmetric anisotropic exchanges that were expected in terms of the original pseudo-spins.

This is an accident of the strict  $j = 1/2$  limit<sup>22</sup>; the symmetric anisotropies, such as  $\Gamma_{zz}$  introduced by tetragonal distortion, the pseudo-dipolar  $K$  or the inter-layer anisotropies in the bilayer case will not be removed. These break the pseudo-SU(2) symmetry and thus set a preferred direction or set of directions in pseudo-spin space. An appropriate choice of these terms<sup>22</sup> can pin the moment in a direction that is staggered following the octahedral rotations as is found in  $\text{Sr}_2\text{IrO}_4$ . The case of  $\text{Sr}_3\text{Ir}_2\text{O}_7$  is less clear, though the moment orientation being very different is not surprising in light of the above discussion. However, it is likely this compound lies far from pseudo-SU(2) invariant limit given the very large gap seen in the spin-wave spectrum<sup>29</sup>. While consensus has not yet been reached, several proposals have put forth mechanisms to explain this collinear order by including large anisotropic couplings<sup>29,30</sup>.

#### D. Topological phases

While in the above sections we started from the Mott insulating limit, in moving to orthorhombic  $\text{SrIrO}_3$  we will start from the itinerant limit. As bulk  $\text{SrIrO}_3$  is a semi-metal with large SOC, variants of this compound may be a good place to look for topological insulators or metals. A band insulator is deemed a topological insulator (TI), if it cannot be smoothly deformed into a decoupled, atomic insulator in such a way that preserves time-reversal symmetry<sup>31,32</sup>. In two or three dimensions this classification into trivial and non-trivial is complete without any further subdivisions<sup>31,32</sup>. TIs have a number of very interesting properties such as gapless edge states and unusual magneto-electric response<sup>31,32</sup>. As discussed in the introduction, most examples of TIs are found in weakly correlated systems. Some proposals have been put forward to look for TIs in transition metal oxides (TMOs): these promise to not only be more robust, but provide a playground to explore the effects of interactions on such topological phases<sup>1,33</sup>.

Among the iridates, it was suggested that  $\text{Na}_2\text{IrO}_3$  could realize a TI with the pseudo-spin  $j = 1/2$  band acquiring a non-trivial  $Z_2$  topological index<sup>34</sup>. While there were some early attempts at explaining the magnetism of  $\text{Na}_2\text{IrO}_3$  within a band-type picture<sup>35</sup>, experimentally it appears that  $\text{Na}_2\text{IrO}_3$  is a Mott insulator. In three dimensions, the pyrochlore iridates were also put forth as candidates to realize a strong TI<sup>1</sup>. Another promising approach is to design the materials of interest by adopting techniques developed in studies of oxide heterostructures<sup>36</sup>. These methods allow for a wide variety of lattice geometries with a greater control over structural distortions and impurity content than is available in bulk samples. Heterostructures built from  $4d$  or  $5d$  TMOs, with their large intrinsic SOC, are thus likely to offer new and interesting phases for study.

A simple example of such physics can be illustrated via bilayers of  $\text{SrIrO}_3$  grown along the  $[111]$  direction<sup>37,38</sup>. In these bilayers the Ir atoms form a buckled honeycomb lattice of corner-shared octahedra, as shown in Fig 4a. As in the proposals to realize a TI in  $\text{Na}_2\text{IrO}_3$ , we have an

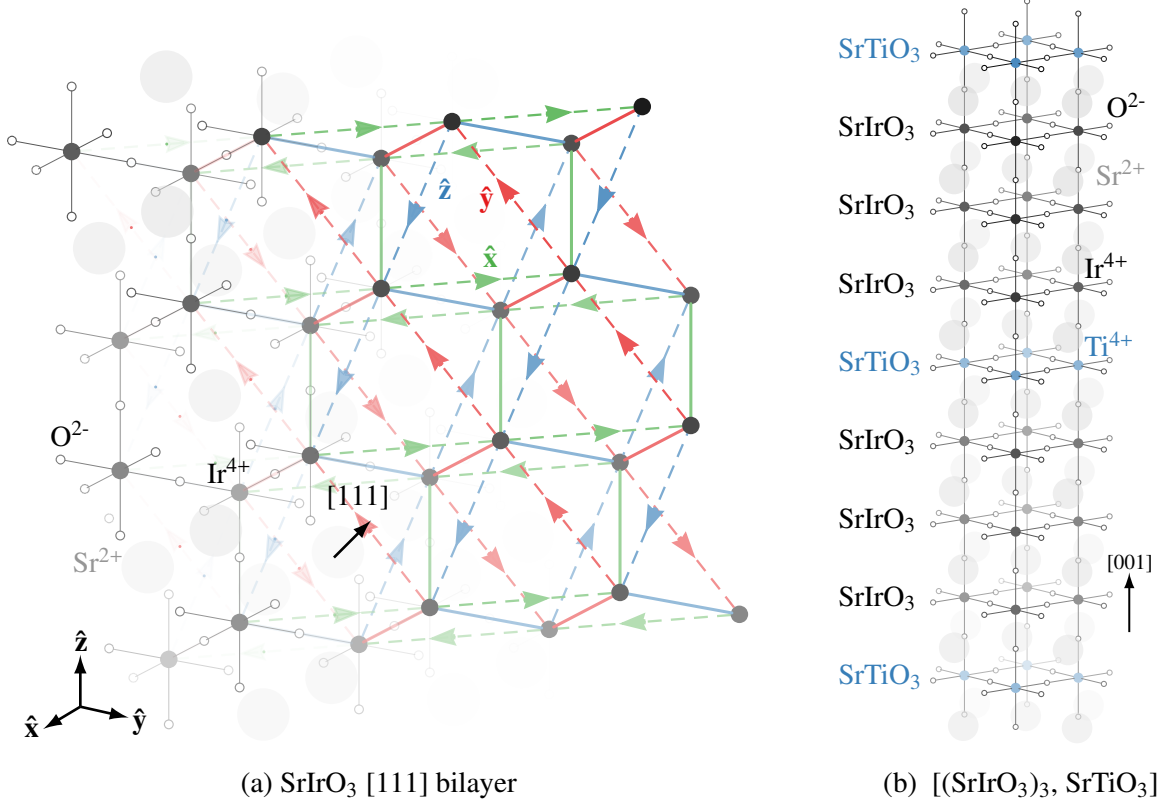


FIG. 4: (a) An ideal bilayer of SrIrO<sub>3</sub> showing the honeycomb lattice formed by the Ir ions. First nearest neighbours are shown by solid lines while second nearest-neighbour bonds are dashed. The arrow indicates the hopping direction, while the colour indicates whether  $\hat{\mathbf{d}}_{ij} = \hat{\mathbf{x}}, \hat{\mathbf{y}}$  or  $\hat{\mathbf{z}}$ . (b) An ideal superlattice [(SrIrO<sub>3</sub>)<sub>3</sub>, SrTiO<sub>3</sub>] along the [001] direction.

itinerant  $j = 1/2$  model of the form

$$-t \sum_{\langle ij \rangle} \sum_{\alpha} (c_{i\alpha}^{\dagger} c_{j\alpha} - \text{h.c.}) + t' \sum_{\langle\langle ij \rangle\rangle} \sum_{\alpha\beta} [c_{i\alpha}^{\dagger} (\boldsymbol{\sigma}_{\alpha\beta} \cdot \hat{\mathbf{d}}_{ij}) c_{j\beta} + \text{h.c.}] + \epsilon \sum_{i\alpha} (-1)^i c_{i\alpha}^{\dagger} c_{i\alpha}, \quad (9)$$

where  $c_{i\alpha}^{\dagger}$  is a creation operator of  $j = 1/2$  electron with the pseudo-spin  $\alpha \equiv j_z = \pm 1/2$  at site  $\mathbf{r}_i$ . The sums over  $\langle \dots \rangle$  and  $\langle\langle \dots \rangle\rangle$  denote the nearest neighbour (NN) and next nearest neighbour (NNN) bonds, respectively. On the NNN bonds the absence of inversion symmetry allows pseudo-spin dependent terms to appear parametrized by  $\hat{\mathbf{d}}_{ij} = \hat{\mathbf{x}}, \hat{\mathbf{y}}$  or  $\hat{\mathbf{z}}$  as illustrated in Fig. 4a. Due to the buckling of the honeycomb lattice, there is an atomic potential  $\epsilon$  staggered between the two sublattices. With  $t' = \epsilon = 0$ , this system is a semi-metal with Dirac cones, as in graphene, while finite  $t'$  or  $\epsilon$  gaps out these cones giving a band insulator. When the atomic potential is sufficiently small, this model supports a TI with a non-trivial  $Z_2$  index and the associated gapless edge modes.

The simple example presented above only begins to scratch the surface of what is possible in these types of engineered systems. One particular class of system that has been systematically studied is a series of artificial superlattices [(SrIrO<sub>3</sub>) <sub>$m$</sub> , SrTiO<sub>3</sub>] where  $m$  is integer, grown along the [001]-axis atop a substrate SrTiO<sub>3</sub>.<sup>23</sup> These superlattices consist of atomically thin slices of

$\text{SrIrO}_3$  separated by layers of insulating  $\text{SrTiO}_3$ . While bulk  $\text{SrIrO}_3$  forms a post-perovskite structure under ambient conditions<sup>9</sup>, when prepared in thin films<sup>39</sup> or superlattices<sup>23</sup>, the  $\text{SrTiO}_3$  layers stabilize the orthorhombic perovskite structure. By tuning the number of  $\text{IrO}_2$  layers, an insulator was achieved for  $m = 1$  single and  $m = 2$  bilayer superlattices, and trilayer  $m = 3$  illustrated in Fig. 4b sits at the verge of MIT driven by the layer number  $m$ <sup>23</sup>. While these  $m = 1$  and  $m = 2$  superlattices are topologically trivial  $j = 1/2$  insulators, a theoretical study on single and bilayer  $\text{SrIrO}_3$  interleaved with a band insulator with orthorhombic perovskite structure (such as  $\text{GdScO}_3$ ,  $\text{CaTiO}_3$ ,  $\text{SrZrO}_3$  or  $\text{SrHfO}_3$ ) suggests a rich phase diagram including topological magnetic insulators, topological crystalline insulators and topological valley insulators<sup>40</sup>.

The stability of some topologically protected states hinges the presence of symmetries. A richer topological classification has been recently uncovered by considering the phases protected by the spatial symmetries of the crystal. These *topological crystalline insulators* share many of the same features as  $Z_2$  TIs, such as protected gapless surface states<sup>41</sup>. In contrast, in the prototypical Weyl semi-metal,<sup>42</sup> the gapless surface states remain protected even in the absence of any symmetry. Given the finer classification that exists for insulators, one can ask if there are topological *metals* that are protected by spatial symmetries. A large class of such topological metals have since been classified<sup>33</sup>; these go beyond the Weyl semi-metal and have surface states protected by either global symmetries or crystal lattice symmetries, or combination of the two. Depending on the symmetry properties and the dimension of the Fermi surface, these surface states can form Dirac cones, flat bands or Fermi arc states.<sup>43</sup> Among the iridates, the three dimensional perovskite iridates  $\text{AIrO}_3$  with A an alkaline earth metal have been recently proposed as an example of topological metals protected by spatial symmetries. These *topological crystalline metals* are analogous to the topological crystalline insulators, with crystal symmetry responsible for the protected surface states.<sup>44</sup> While the bulk states show a nodal of ring of gapless excitations, protected by time-reversal and spatial symmetries, the associated two-dimensional surface states are flat in one direction, while linearly dispersing in the other. If one adds external symmetry breaking terms such as those that break time-reversal, mirror, or glide symmetry, this topological metal acts as a seed for a rich family of topological phases, such as a Weyl semi-metal, strong or weak topological insulator, or topological magnetic insulator<sup>44</sup>.

### E. Superconductivity

We now return to the original motivation for the study of the iridates and  $\text{Sr}_2\text{IrO}_4$  in particular: possible links to the physics of high-temperature superconductivity<sup>45</sup> and the realization of exotic superconducting pairing symmetry<sup>46</sup> in doped spin-orbit Mott insulators. In multi-orbital systems it is a challenge to understand the role played by the orbital degrees of freedom in the microscopic mechanism of superconductivity. The superconductor  $\text{Sr}_2\text{RuO}_4$  provides a relevant example, with all three  $t_{2g}$  orbitals important in constructing Fermi surface. Even such a  $4d$  transition metal SCs with intermediate SOC, multi-orbital interactions such as Hunds coupling can be important.<sup>3</sup>

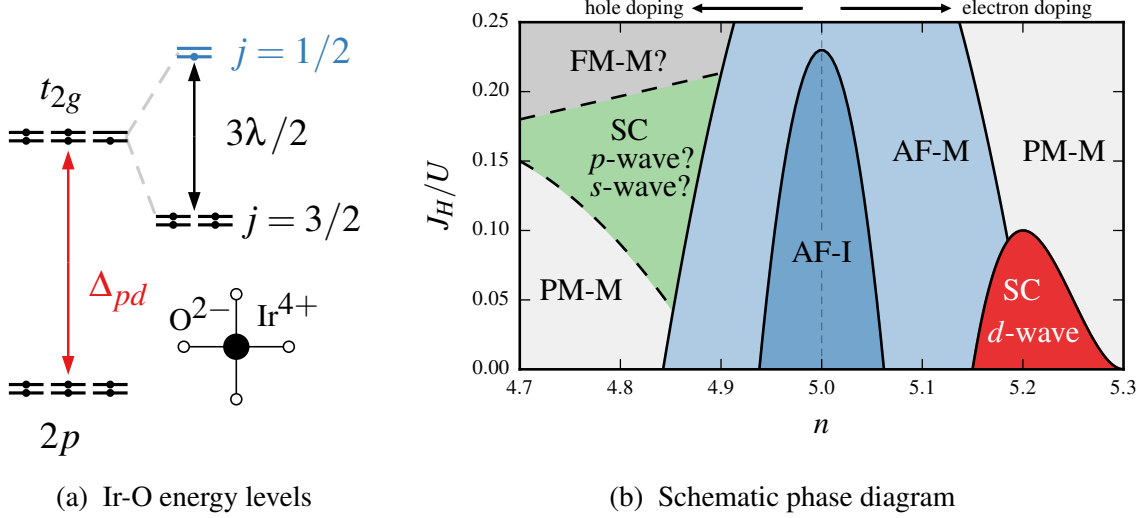


FIG. 5: (a) An illustration of the energy levels for the iridium and oxygen atoms. A hole on the oxygen is more costly than one in the  $j = 3/2$  states. (b) Schematic phase diagram for  $\text{Sr}_2\text{IrO}_4$  as a function of filling  $n$  and Hund's coupling  $J_H$ , based on Ref. [47]. A variety of phases appear such as an antiferromagnetic insulator (AF-I) and metal (AF-M), a paramagnetic metal (PM-M), a ferromagnetic metal (FM-M) as well as possibly two distinct superconducting (SC) phases.

Moving to 5d transition metals, the large SOC can no longer be ignored and the system may display a complex combination of spin-singlet and spin-triplet SC order parameters. As the SOC and other electronic interactions such as Hund's coupling become comparable, the determination of the ground states in such multi-orbital systems is highly non-trivial. In particular, we will discuss how the physics of doping in  $\text{Sr}_2\text{IrO}_4$  is both similar to, but different from the case of cuprate superconductors. We then discuss some recent theoretical work that explore possible pairing symmetries and mechanisms for superconductors arising from doped Mott insulators with strong SOC. From there, we review the on-going experimental search for superconductivity in doped iridates, focusing in particular on progress in doping  $\text{Sr}_2\text{IrO}_4$ .

The physics of doping electrons into these  $j = 1/2$  Mott insulators is familiar. Given the filled 2p orbitals of the neighbouring oxygens and the filled  $j = 3/2$  states, the least costly place to put an extra electron is in the  $j = 1/2$  states themselves. The penalty is the Coulomb energy  $U$ ; much smaller than filling any of the higher-lying electronic states. We caution that this is purely at the atomic level and electronic structure effects can alter this identification. For example for  $\text{Sr}_2\text{IrO}_4$  it has been argued that the electron doping is similar to the hole-doped cuprates due to an opposite sign in the next-nearest neighbour hopping integral<sup>28</sup>. However when iridates are hole-doped, the multi-orbital nature can become active and it may not be this simple. The key distinction is in the energy gap to the nearest 5d states, the  $j = 3/2$  levels. In the cuprates, tetragonal distortion separates the ground state doublet from the nearest 3d levels by a gap of  $\sim 1-2$  eV<sup>48</sup>. This is larger or comparable to the cost of putting the hole onto the neighbouring oxygens once hybridization

effects are taken into account. In the case of the iridium oxides the  $j = 3/2$  states are only  $\sim 0.5$  eV away while the oxygens are  $\sim 1 - 2$  eV. It is then favourable to put the hole not on the oxygens, but on  $\text{Ir}^{4+}$  itself in the  $j = 3/2$  states. Hund's coupling between the  $j = 1/2$  and  $j = 3/2$  states can further stabilize these holes. This is schematically summarized in Fig. 5a. A single-orbital  $j = 1/2$  picture, enabled by the formation of a Zhang-Rice singlet, may no longer be tenable and one must move beyond a  $t$ - $J$  type model and include aspects of the full multi-orbital problem. This can be seen clearly in how these same  $j = 3/2$  excited states appear in the localized spin model for the half-filled  $d^5$  case, where they generate bond-dependent exchanges as discussed in Sec. III B and will be essential in Sec. IV.

The classification of pairing terms is also modified when SOC is strong; as spin is no longer a conserved quantity spin-singlet or spin-triplet lose their meaning. However a version of this can be recovered if the strong SOC leads to a single FS with  $j = 1/2$  character and the multi-orbital problem can be reduced to an effective single band model. If the pseudo-spin dependent terms can be made small, one can define effective pseudo-spin-singlet and pseudo-spin-triplet SC pairing symmetries. This assumption is likely valid in  $\text{Sr}_2\text{IrO}_4$ , where most of FS is of  $j = 1/2$  character and the nearest-neighbour pseudo-spin dependent terms can be absorbed into the definition of the  $j = 1/2$  states<sup>5</sup>. Given the similarity in lattice structure and Mott physics between  $\text{Sr}_2\text{IrO}_4$  and  $\text{La}_2\text{CuO}_4$ , it was proposed that a pseudo-spin-singlet  $d$ -wave high temperature SC phase like cuprates may emerge in electron-doped iridates.<sup>28</sup> As discussed above, the hole-doped case may be significantly different due to the competition between Hund's coupling and SOC. With finite Hund's coupling one may expect an effective interaction through the exchange of ferromagnetic pseudo-spin fluctuations. So long as the Hund's coupling is not so large as to drive the system into a ferromagnetic state, one then would expect to generate a pseudo-spin triplet pairing. Indeed, recent large-scale dynamical mean-field theory calculations support such a picture. In these simulations a  $d$ -wave pseudo-spin-singlet SC was found on the electron-doped side, while a topological  $p + ip$ -wave pseudo-spin-triplet SC was found on the hole doped side<sup>47</sup>. These may be relevant for hole-doped  $\text{Sr}_2\text{IrO}_4$ , or possibly even  $\text{Sr}_2\text{RuO}_4$ . A schematic phase diagram as a function of doping and Hund's coupling is shown in Fig. 5b.

Experimental studies on physics of doping holes or electrons into  $\text{Sr}_2\text{IrO}_4$  have been carried out through a variety of means; these include electron doping through depleting oxygen<sup>49</sup>, La-substitution<sup>50,51</sup>, or surface doping<sup>52</sup> as well as hole-doping through substitution of Rh for Ir<sup>50,53</sup>. While SC has not been discovered, in each case modest doping suppresses the magnetic and strongly affects transport. Doping the bilayer  $\text{Sr}_3\text{Ir}_2\text{O}_7$  with 5% La induces a robust metallic state, with the resistivity showing a rapid drop below 20 K. The magnetic order remains finite despite strong suppression of  $T_c$ <sup>54</sup>. This is in contrast to the case of La-doped  $\text{Sr}_2\text{IrO}_4$ , where the magnetic order is completely suppressed in the metallic state.<sup>51</sup> In addition to the transport and magnetic properties, angle resolved photoemission spectroscopy (ARPES) provides interesting insights into physics of the doped iridates. It was reported that Rh-doped  $\text{Sr}_2\text{IrO}_4$  exhibits a pseudo gap and Fermi arcs<sup>53</sup> similar to the doped cuprates. Similar Fermi arcs were also found in surface electron doped  $\text{Sr}_2\text{IrO}_4$ <sup>52</sup> along with the anomalous waterfall-like feature in the ARPES spectra<sup>55</sup>. Though



similar Fermi arc-like features observed in La-doped  $\text{Sr}_3\text{Ir}_2\text{O}_7$ , have been attributed to Fermi pockets masked by matrix element effects<sup>56</sup>, this does not explain the temperature dependence of the Fermi arcs in Ref. [52], suggesting a different origin.

#### IV. SPIN LIQUIDS AND UNCONVENTIONAL MAGNETIC ORDERS IN HONEYCOMB IRIDATES

Despite tremendous efforts, the search for a quantum spin liquid in a real material remains unresolved. A significant amount of attention in this search has been directed towards geometrically frustrated antiferromagnets, such as those on Kagomé or triangular lattices. Many of these systems are described by Heisenberg-like models, possibly extended with ring exchange terms or with small anisotropies. While some candidates exist, the combination of theoretical and experimental uncertainties has made definite confirmation of the spin liquid state difficult. A promising approach to circumvent some of these theoretical difficulties is based on Kitaev's exactly solvable honeycomb model<sup>57</sup>. This highly anisotropic compass model<sup>58</sup> is frustrated not by the geometry of the lattice, but by the intertwining of spatial and spin degrees of freedom. One can generalize this approach, defining such exactly solvable models on trivalent lattices in two or three dimensions. The presence of the solvable point present in the model then provides a controlled starting point to study the stability of the spin liquid and possible nearby unusual ordered phases. The challenge is then to find materials that implement these models.

Here we discuss possible realizations of these Kitaev-type models in Mott insulators with strong SOC. In two dimensions, there are the well-studied honeycomb iridates  $\text{Na}_2\text{IrO}_3$  and  $\alpha\text{-Li}_2\text{IrO}_3$ , which host magnetically ordered phases thought to be proximate to the spin liquid phase; and the honeycomb ruthenium chloride  $\alpha\text{-RuCl}_3$ , which has been recently proposed as a  $4d$  analogue. Two three-dimensional lattices have also been synthesized in polymorphs of the honeycomb  $\alpha\text{-Li}_2\text{IrO}_3$ . These are the hyper-honeycomb  $\beta\text{-Li}_2\text{IrO}_3$  and stripy-honeycomb  $\gamma\text{-Li}_2\text{IrO}_3$ . First, we start with an overview of their shared basic physics: edge-shared octahedra.

##### A. Spin-orbit Mott insulators with edge-shared octahedra

Finding a system that realizes Kitaev's honeycomb model or its analogues is difficult; no symmetry principle prevents the introduction of other interactions, such as Heisenberg exchange<sup>59</sup>. The best one can hope for is the *dominance* of Kitaev exchanges among symmetry allowed interactions. One route to achieve this was introduced in the pioneering work of Jackeli and Khaliullin<sup>22</sup> based on spin-orbit entangled pseudo-spins in a  $90^\circ$  bonding geometry. This provides a natural mechanism to generate bond-dependent Ising interactions<sup>2</sup>, the building block of the Kitaev model. For concreteness, we discuss this in the context of iridium oxides, but translation to related compounds such as  $\alpha\text{-RuCl}_3$  is straightforward.

In contrast to the perovskite iridates discussed in Sec. III, we consider materials where the oxy-



gen octahedra of neighbouring iridium atoms share an *edge*, rather than a corner. In addition, these materials are farther from the itinerant limit discussed for the perovskite case, lying firmly in the Mott regime. We assume that the dominant exchange pathways between iridium  $5d$  orbitals proceed through the oxygen  $2p$  orbitals with a large gap  $\Delta_{dp}$  between the  $5d$  and  $2p$  states. Integrating out these oxygen states yields an effective inter-orbital hopping  $t \equiv t_{pd\pi}^2/\Delta_{dp}$  with  $t_{pd\pi}$  being the Slater-Koster  $\pi$ -overlap and between the  $5d$  and  $2p$  orbitals. The pair of  $5d$  orbitals linked depends on the edge shared;  $d_{yz}$  and  $d_{xz}$  orbitals mix on  $z$ -links,  $d_{yz}$  and  $d_{xy}$  on  $y$ -links and  $d_{xz}$  and  $d_{xy}$  on  $x$ -links, as shown in Fig. 6. To understand the Mott insulating phase we will consider the effective model in the strong coupling limit where  $U, J_H, \lambda \gg t$ , which can be expressed entirely in terms of the  $j = 1/2$  pseudo-spins. The simplest approach is to first project the multi-orbital model of Eq. (2) into isolated  $j = 1/2$  bands prior to taking the strong-coupling limit, as was done in Sec. III B. One finds that the inter-orbital hoppings  $t$  *vanish* when projected into the  $j = 1/2$  bands, and thus no exchange is generated. Similarly, even in the full multi-orbital problem, no exchange arises when Hund's coupling is absent. These results suggest that in this case the complete multi-orbital nature of the problem must be considered to account for the interactions between the  $j = 1/2$  spins. To include both the  $j = 3/2$  virtual states and the effects of Hund's coupling, one must use a more realistic limit where  $U, J_H \gg \lambda$  or  $U, \lambda \gg J_H$ , obtaining an effective interaction of Kitaev type<sup>22</sup>

$$\sim -\frac{8t^2 J_H}{3U^2} J_1^\gamma J_2^\gamma, \quad (10)$$

where  $\gamma$  indicates the type of edge shared by the neighbouring  $j = 1/2$  spins  $\mathbf{J}_1$  and  $\mathbf{J}_2$ .

This Hamiltonian is only applicable when the oxygen mediated processes are dominant and  $\Delta_{dp}$  is very large. If other hopping interactions such as direct  $5d$ - $5d$  overlap<sup>60</sup> or other super-exchange pathways<sup>60,61</sup> are included, then one expects all symmetry allowed terms to be generated. For a pair of ideal edge-shared octahedra, the bond symmetry allows two additional terms: a Heisenberg interaction  $J$  and a symmetric off-diagonal exchange  $\Gamma$ <sup>62</sup>. An effective exchange model for the pair of spins is then

$$J\mathbf{J}_1 \cdot \mathbf{J}_2 + KJ_1^\gamma J_2^\gamma + \Gamma(J_1^\alpha J_2^\beta + J_1^\beta J_2^\alpha), \quad (11)$$

where  $\alpha, \beta$  indicate the two spin directions not equal to the edge-type  $\gamma$ . If we assume the exchange physics is local to the pair of octahedra, then fixing the parameters on one edge is sufficient to determine the others related by symmetry. Details of the dependence of  $J, K$  and  $\Gamma$  on the atomic interactions for two of the limiting schemes described here can be found in Rau *et al.*<sup>62</sup>.

## B. Distortions

The crystal structure of the honeycomb compounds  $\text{Na}_2\text{IrO}_3$  and  $\alpha\text{-Li}_2\text{IrO}_3$ , and the three-dimensional analogues  $\beta\text{-Li}_2\text{IrO}_3$  and  $\gamma\text{-Li}_2\text{IrO}_3$  deviate from this idealized picture due to the presence of trigonal and monoclinic distortions. Following the discussion in Section III C, for trigonal distortion, in Eq. (6) one has  $\hat{\mathbf{n}} \equiv (\hat{\mathbf{x}} + \hat{\mathbf{y}} + \hat{\mathbf{z}})/\sqrt{3}$  or one of its equivalents. In the absence

of SOC, this splits the  $t_{2g}$  levels into an  $a_{1g}$  singlet and  $e_g$  doublet. When SOC is present, the highest-lying Kramers doublet connects to the  $j = 1/2$  states and can be found explicitly in Ref. [2]. Monoclinic distortion cannot lift the degeneracy any further, but will complicate the structure and analysis of these ground state wave-functions. Corrections to interactions between the  $j = 1/2$  spins will be introduced through these changes in the atomic wave-functions, as well as through the kinetic parts of the exchange processes which depend on the geometry of the oxygen ions.

Rather than attempt to connect the details of the distortions to the exchange interactions directly, we consider the new interactions allowed by these reductions of symmetry. In the materials under consideration, there are two or more symmetry inequivalent sets of nearest-neighbour bonds, one with higher symmetry and the rest with lower symmetry. The higher bond symmetry groups are 222 for  $\beta$ -Li<sub>2</sub>IrO<sub>3</sub> and  $\gamma$ -Li<sub>2</sub>IrO<sub>3</sub> and  $2/m$  for  $\alpha$ -Li<sub>2</sub>IrO<sub>3</sub> and Na<sub>2</sub>IrO<sub>3</sub>. For a bond with  $2/m$  symmetry, the allowed exchanges include those in Eq. (11) but with an additional symmetric off-diagonal exchange

$$\Gamma' \left( J_1^\alpha J_2^\gamma + J_1^\beta J_2^\gamma + J_1^\gamma J_2^\alpha + J_1^\gamma J_2^\beta \right). \quad (12)$$

As an example, trigonal distortion of the oxygen octahedra can introduce such a term<sup>63</sup>. For a bond with 222 symmetry, such a term is forbidden, but due to the lack of inversion about the bond center an analogous DM interaction is allowed

$$D \left( J_1^\alpha J_2^\gamma + J_1^\beta J_2^\gamma - J_1^\gamma J_2^\alpha - J_1^\gamma J_2^\beta \right). \quad (13)$$

The lower symmetry bonds of  $\alpha$ -Li<sub>2</sub>IrO<sub>3</sub>,  $\beta$ -Li<sub>2</sub>IrO<sub>3</sub>, and Na<sub>2</sub>IrO<sub>3</sub> have only inversion about the bond center while that of  $\gamma$ -Li<sub>2</sub>IrO<sub>3</sub> has no symmetry at all. In the compounds with an inversion, this implies the absence of DM interaction on these bonds.

Further neighbour exchange interactions can be analyzed in a similar fashion, though the number of allowed interactions grows quickly. These are thought to be important<sup>64–67</sup> in Na<sub>2</sub>IrO<sub>3</sub> where the Mott gap is not too large<sup>68</sup>. Some discussion of the symmetry allowed interactions in Na<sub>2</sub>IrO<sub>3</sub> for second and third nearest neighbours can be found in Yamaji *et al.*<sup>66</sup> and Sizyuk *et al.*<sup>67</sup>. While there has been some work on further neighbour interactions in the three-dimensional compounds<sup>69,70</sup>, their effects and importance remain largely unaddressed.

### C. Kitaev physics in two dimensions

With this framework in hand, we first turn to possible realizations of Kitaev's two-dimensional honeycomb model. Promising candidates thought to be proximate to this physics are the honeycomb iridates Na<sub>2</sub>IrO<sub>3</sub> and  $\alpha$ -Li<sub>2</sub>IrO<sub>3</sub>, and more recently,  $\alpha$ -RuCl<sub>3</sub>. These materials do *not* have a spin liquid ground state, but instead order magnetically as temperature is lowered. To understand if the proximity to Kitaev physics is governing their behaviour we first study these magnetic phases.

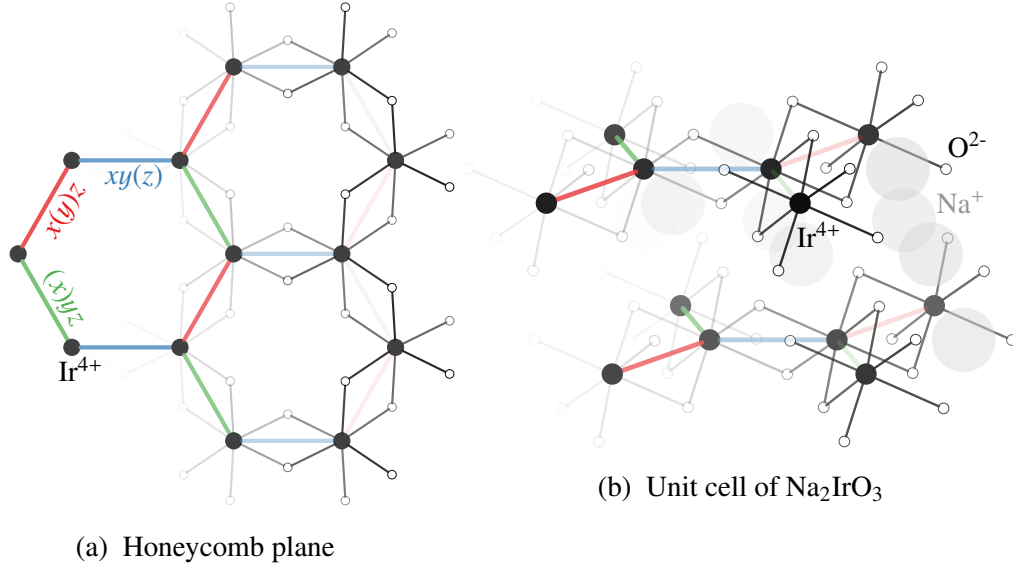


FIG. 6: Crystal structure of the layered  $\text{Na}_2\text{IrO}_3$ . (a) The unit cell of  $\text{Na}_2\text{IrO}_3$  showing the quasi-two dimensional layered structure. (b) The honeycomb plane of  $\text{Na}_2\text{IrO}_3$  showing the labeling of the nearest neighbour bonds, with a  $\gamma = x, y, z$  type bond labeled as  $\alpha\beta(\gamma)$ .

### 1. Experimental review

The crystal structures of these compounds (see Fig. 6) takes the form of layers of edge-shared  $\text{IrO}_6$  octahedra arranged in a honeycomb lattice<sup>71,72</sup>. These octahedra are compressed in the direction perpendicular to the honeycomb planes, with further monoclinic distortions along a preferred axis<sup>73,74</sup>. A 340 meV optical gap<sup>68</sup> and estimates of  $3\lambda/2 \sim 0.5$  eV<sup>75</sup> for SOC identify  $\text{Na}_2\text{IrO}_3$  as a candidate for a  $j = 1/2$  spin-orbit Mott insulator. Fits of the magnetic susceptibility confirm the effective spin-1/2 picture, giving a magnetic moment  $\sim 1.82\mu_B$  with large antiferromagnetic Curie-Weiss temperature  $\theta_{\text{CW}} \sim -116$  K<sup>71</sup>. The low temperature antiferromagnetic ordering transition seen near  $T_N \sim 15$  K suggests substantial frustration. Neutron scattering and resonant X-ray scattering studies<sup>73,74,76</sup> have unambiguously identified this ordering as having a *zigzag* structure. This zigzag order consists of spins aligned ferromagnetically along one direction, with the chains alternating antiferromagnetically as illustrated in Fig. 7. Dynamical probes, such as inelastic neutron scattering (INS) and resonant inelastic X-ray scattering (RIXS), have provided additional clues via access to their excitations. RIXS studies have shown<sup>77</sup> that there is a branch of magnetic excitations at high-energy near  $\sim 30$  meV. Though some dispersion can be identified, any information about the excitations below  $\sim 10$  meV is lost due to limitations in energy resolution. INS studies offer a complementary picture, but due to the large neutron absorption cross-section of Ir, they have been limited to powder samples<sup>74</sup> providing a higher energy resolution but only a few details of the distribution in wave-vector. Nonetheless, below the Néel temperature, two key features can be resolved: scattering near the magnitude of the zigzag ordering wave-vector is present down to at least 2 meV and there is an absence of scattering at small wave-vectors and energy. Re-

cent diffuse magnetic X-ray scattering<sup>78</sup> in the paramagnetic phase has provided an experimental confirmation of dominant Kitaev interactions, validating the theoretical arguments of Sec. IV A. These measurements show a clear locking of the spatial and spin orientations characteristic of the bond-dependent Kitaev exchange. For  $\alpha$ -Li<sub>2</sub>IrO<sub>3</sub> the situation is less clear. Experimentally, an antiferromagnetic ordering transition<sup>72</sup> is seen at  $\sim 15$  K, as in Na<sub>2</sub>IrO<sub>3</sub>, but  $\alpha$ -Li<sub>2</sub>IrO<sub>3</sub> has a smaller Curie-Weiss temperature of  $\theta_{\text{CW}} \sim -33$  K. While there have been reports of an incommensurate ordering wave vector lying in the first Brillouin zone<sup>79</sup>, the details of the magnetic ordering pattern and the structure of the low energy excitations remain largely unresolved.

A number of studies have tried to elucidate the properties of these materials more indirectly through elemental substitution. One promising approach is to dope isoelectronically from Na<sub>2</sub>IrO<sub>3</sub> to  $\alpha$ -Li<sub>2</sub>IrO<sub>3</sub> as (Na<sub>1-x</sub>Li<sub>x</sub>)<sub>2</sub>IrO<sub>3</sub>. For  $x \lesssim 0.25$ , uniform solid solutions can be obtained, with both  $T_N$  and  $|\theta_{\text{CW}}|$  suppressed with increased doping<sup>80,81</sup>. While a quantum critical point near  $x_c \sim 0.75$  was found in Ref. [80], indications of phase separation reported for the range  $0.25 \lesssim x \lesssim 0.6$ <sup>81</sup> complicate this identification. Further study is needed for  $x \gtrsim 0.6$  near the  $\alpha$ -Li<sub>2</sub>IrO<sub>3</sub> end of this range to clarify the issue. Another approach is dilution of Ir<sup>4+</sup> with non-magnetic Ti<sup>4+</sup><sup>82</sup>, forming Na<sub>2</sub>(Ir<sub>1-x</sub>Ti<sub>x</sub>)O<sub>3</sub> or Li<sub>2</sub>(Ir<sub>1-x</sub>Ti<sub>x</sub>)O<sub>3</sub>. As the magnetic lattice of Ir is depleted, both systems enter a spin-glass phase, consistent with the high frustration indicated by  $T_N/|\theta_{\text{CW}}|$ . In both compounds the spin glass ordering temperature  $T_g$  decreases roughly linearly as a function of  $x$  until to the site-percolation threshold at  $x_p \sim 0.3$ . These two cases are distinguished by the dependence of the Curie-Weiss temperature on dilution: the Na<sub>2</sub>(Ir<sub>1-x</sub>Ti<sub>x</sub>)O<sub>3</sub> shows a marked decrease as  $x$  is increased while for the Li<sub>2</sub>(Ir<sub>1-x</sub>Ti<sub>x</sub>)O<sub>3</sub> it is essentially constant. This has been interpreted<sup>82</sup> as evidence of more significant long range interactions in  $\alpha$ -Li<sub>2</sub>IrO<sub>3</sub> compared to Na<sub>2</sub>IrO<sub>3</sub>.

## 2. Theory

The balance of experimental evidence has suggested that large Kitaev interactions are necessary to understand the physics of Na<sub>2</sub>IrO<sub>3</sub> and  $\alpha$ -Li<sub>2</sub>IrO<sub>3</sub>. However, the low-energy physics and the ground state selection are dependent on the details of the perturbations that take us away from the Kitaev limit. These questions have led to a number of theoretical proposals that have been put forth to explain the appearance of zigzag ordering in Na<sub>2</sub>IrO<sub>3</sub> and the nature of the magnetic ordering in  $\alpha$ -Li<sub>2</sub>IrO<sub>3</sub>.

Early work on Na<sub>2</sub>IrO<sub>3</sub><sup>60</sup> primarily focused on the Heisenberg-Kitaev (HK) model and its extensions. In the HK model, the Kitaev exchange is supplemented by a conventional Heisenberg interaction

$$\sum_{\langle ij \rangle \in \gamma} (J \mathbf{J}_i \cdot \mathbf{J}_j + K S_i^\gamma S_j^\gamma). \quad (14)$$

This model has since attracted much theoretical attention, not only due to its relation to the honeycomb iridates, but also as a model system to study the stability of the Kitaev spin liquid and its neighboring phases<sup>83–87</sup>. The remainder of the phase diagram of this model can be understood almost completely with the help of a four-sublattice spin rotation—the so-called *Klein duality*. This

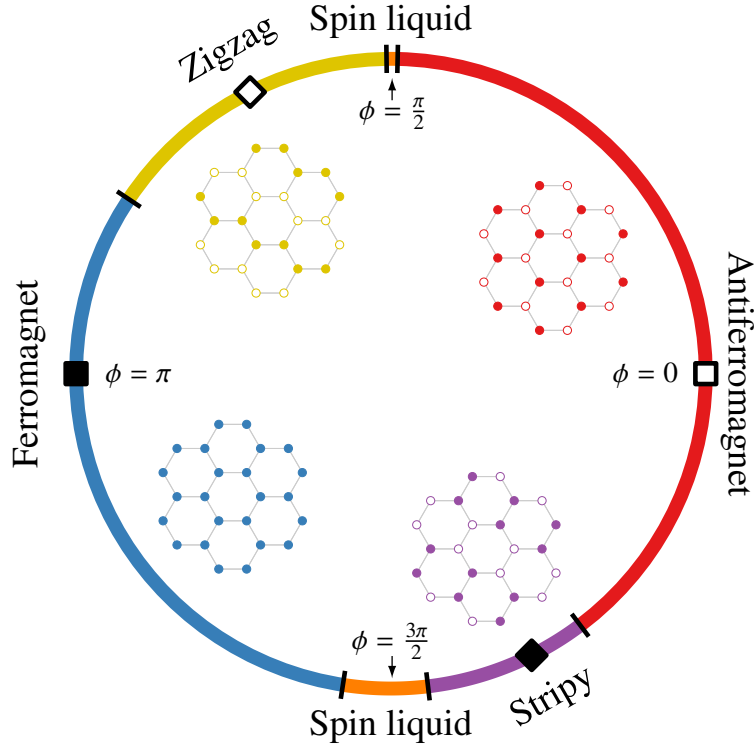


FIG. 7: Phase diagram of the Heisenberg-Kitaev model. The model is parametrized as  $J = \cos \phi$ ,  $K = \sin \phi$ , as discussed in the main text. Squares and diamonds show points related by the Klein duality transformation. Phases of the Heisenberg-Kitaev model are shown inside, these are the ferromagnet (FM), antiferromagnet (AFM), stripy (ST) and zigzag (ZZ).

duality maps the HK model to itself, but with the modified parameters  $J' = -J$  and  $K' = K + 2J$ . Applying this duality to the ferromagnetic and antiferromagnetic Heisenberg limits yields two new well-understood limits. These are the stripy (ST) phase at  $K = -2J < 0$  dual to the ferromagnet (FM) and the zigzag (ZZ) phase at  $K = 2J > 0$  dual to the antiferromagnet (AFM). These ordered phases are illustrated in Fig 7. The Kitaev spin liquid is stable to finite  $J$  and maps to itself under the Klein duality. These five phases encompass all phases present in the model. This has been borne out using a number of theoretical methods<sup>60,83,84</sup>; the full phase diagram parametrized as  $J = \cos \phi$ ,  $K = \sin \phi$  is presented in Fig. 7.

For the presumed ferromagnetic Kitaev interaction ( $K < 0$ ), the neighboring magnetic phases are a ferromagnet and a stripy phase<sup>60</sup>. It is possible to obtain a zigzag ground state with this model, but only when the Kitaev interaction is antiferromagnetic ( $K > 0$ ) and the Heisenberg interaction is ferromagnetic ( $J < 0$ ). The need for a large antiferromagnetic Kitaev interaction is at odds with expectations from a picture of dominant oxygen-mediated super-exchange. Some efforts have been made to justify<sup>61</sup> this parameter regime, while others<sup>64,72,74</sup> have added additional couplings to the ferromagnetic Kitaev limit in an attempt to resolve the discrepancy. Recent *ab-initio* calculations<sup>65,66</sup> have supported the view that ferromagnetic Kitaev interactions are the proper starting point. Starting from this Kitaev limit, theoretical studies have considered the ef-

fects of the symmetry allowed nearest-neighbour interactions<sup>62,63,65</sup>, such as the  $\Gamma$  from Eq. (11) and  $\Gamma'$  from Eq. (12), as well as further neighbour interactions<sup>66,67</sup>. While the details differ, in all of the above works a zigzag phase can be stabilized near the ferromagnetic Kitaev limit by some combination of further neighbour and anisotropic interactions.

Even with the scarcity of experimental information, several theories have been put forth to explain the possibility of incommensurate ordering in  $\alpha$ -Li<sub>2</sub>IrO<sub>3</sub>. A common approach is to move away from some of the limiting regimes studied for Na<sub>2</sub>IrO<sub>3</sub>. For example, in Ref. [84], the HK model was extended to include second nearest-neighbour Heisenberg and Kitaev exchange interactions. In this regime one can find an incommensurate spiral phase with wave-vector lying in the first Brillouin zone, as has been reported in  $\alpha$ -Li<sub>2</sub>IrO<sub>3</sub>. In Refs. [63] and [88], one perturbs away from the zigzag phase stabilized by anisotropic exchanges  $\Gamma$  and  $\Gamma'$ , which is relevant for Na<sub>2</sub>IrO<sub>3</sub>, to find similar incommensurate phases. Other approaches begin from a more monoclinic limit, considering quasi-one-dimensional chains<sup>70</sup> or strengthening Kitaev interactions on one set of bonds<sup>89</sup>. The lack of details on the reported incommensurate spiral phase coupled with the same large parameter space that plagues Na<sub>2</sub>IrO<sub>3</sub> leaves many questions open for  $\alpha$ -Li<sub>2</sub>IrO<sub>3</sub>.

### 3. $\alpha$ -RuCl<sub>3</sub>

The 4d compound  $\alpha$ -RuCl<sub>3</sub> has recently attracted attention as another possible system to explore Kitaev physics. As in honeycomb iridates, the Ru<sup>3+</sup> ion has a  $d^5$  configuration but with an octahedral cage of Cl<sup>-</sup> rather than O<sup>2-</sup>. These octahedra are then arranged in a layered, edge-shared honeycomb network with space group  $P3_112$ <sup>90</sup>. While first identified as a band insulator<sup>91</sup>, spectroscopic studies<sup>92,93</sup> have since converged to a picture of  $\alpha$ -RuCl<sub>3</sub> as a Mott insulator. Indeed, this is supported by measurements of the magnetic susceptibility, which takes a Curie-Weiss form with an average moment  $\sim 2.0 - 2.3 \mu_B$ , not too far from what would be expected for a spin-1/2<sup>94,95</sup>. Going to lower temperatures, antiferromagnetic order appears near  $\sim 7$  K, as seen in specific heat and magnetic susceptibility measurements<sup>96-98</sup>. Neutron scattering experiments<sup>97,99</sup> have identified this order as being zigzag<sup>97,99</sup> as seen in Na<sub>2</sub>IrO<sub>3</sub>. Further, a broad specific heat feature seen near  $\sim 15$  K<sup>96,97</sup> may be an indication of a multi-step transition process.

While strongly suggestive of the same physics seen in the honeycomb iridates, one may be concerned with the applicability of the  $j = 1/2$  picture itself. Given the considerably smaller SOC in the 4d orbitals of Ru<sup>3+</sup><sup>100</sup>, strong overlap of the  $j = 1/2$  and  $j = 3/2$  bands is possible and would require a more complicated description of the Mott insulating phase. One proposed resolution<sup>101</sup>, motivated by ab-initio calculations, invokes the enhancement of SOC by electronic correlation effects. This SOC enhancement cleanly separates the  $j = 1/2$  states from the  $j = 3/2$  and increases the tendency towards a Mott phase. Several theoretical descriptions<sup>96,99,101</sup> have been put forth to explain the appropriate low-energy physics, as well as the nature of the ordered phase that appears at low temperature.

Some of the key differences between  $\alpha$ -RuCl<sub>3</sub> and the honeycomb iridates may render it a



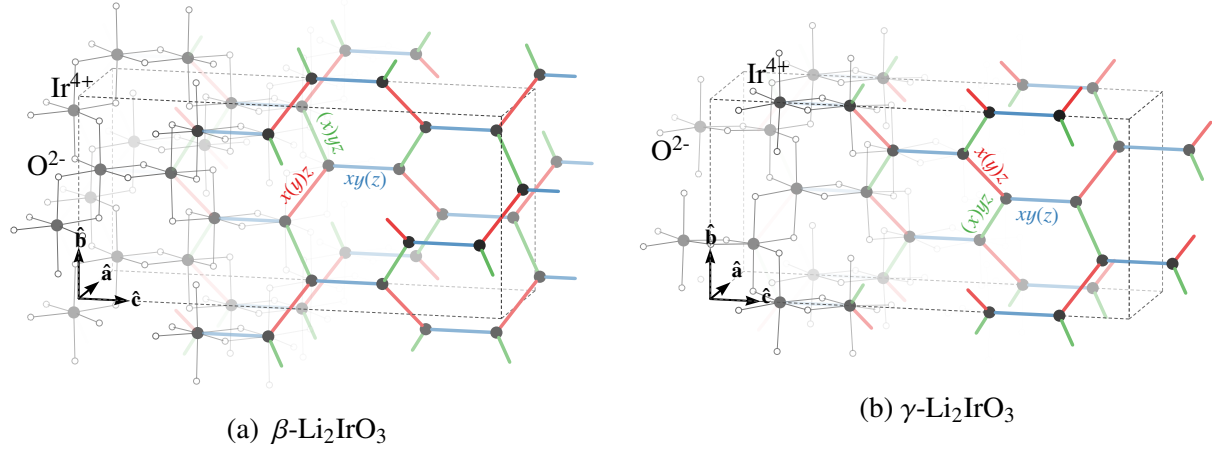


FIG. 8: Crystal structures of the (a) hyper-honeycomb  $\beta$ -Li<sub>2</sub>IrO<sub>3</sub> and the (b) stripy-honeycomb  $\gamma$ -Li<sub>2</sub>IrO<sub>3</sub>. Each structure is formed from a network of approximately edge-shared IrO<sub>6</sub> octahedra, with bonds of type  $\gamma = x, y, z$  labeled as  $\alpha\beta(\gamma)$ .

much better system to study Kitaev magnetism. Indeed, geometrically the local environment of the Ru ion is nearly distortion-free<sup>93,97</sup>, lacking the significant trigonal or monoclinic distortions that have been reported<sup>71,72</sup> in Na<sub>2</sub>IrO<sub>3</sub> and  $\alpha$ -Li<sub>2</sub>IrO<sub>3</sub>. Access to the details of the magnetic excitation spectrum, due to the absence of neutron absorbing Ir atoms<sup>99</sup>, should further illuminate the physics of this material. Aside from pinning down the theoretical description, with more information and fewer parameters it may be easier to perturb the system toward the sought-after Kitaev spin liquid phase<sup>99</sup>.

#### D. Kitaev physics in three dimensions

The search for spin liquids in three dimensional materials has focused on a handful of frustrated lattices, for example on the pyrochlore<sup>102,103</sup> or the hyper-kagome, realized in the iridate Na<sub>4</sub>Ir<sub>3</sub>O<sub>8</sub><sup>104,105</sup>. As in the two-dimensional cases discussed in Section IV have been put forth, the definite confirmation of the spin liquid state remains very challenging both theoretically and experimentally. While further work is warranted, following our discussion in two-dimensions, an alternative route to a three-dimensional spin liquid might lie through an extension of the Kitaev's honeycomb model.

The exact solvability of Kitaev's 2D honeycomb model depends on the three-fold coordination of each site and the appropriate assignment of Ising components among the bonds, *i.e.* the Ising interactions are along the  $x, y$ , or  $z$  directions while bonds with the same Ising components do not share the same site. These properties can be realized on many lattices, hence Kitaev's 2D honeycomb model can be generalized to three-dimensions. One such example is a spin-1/2 model defined on a 3D deleted-cubic lattice, whose exact spin liquid solution and excitations were studied in Ref. [106]. Fortuitously, an iridate material with the Ir ions residing on a topologically-equivalent



lattice was synthesized several years later: the hyper-honeycomb  $\beta$ -Li<sub>2</sub>IrO<sub>3</sub>.<sup>107</sup> Almost simultaneously, another polymorph—the stripy-honeycomb  $\gamma$ -Li<sub>2</sub>IrO<sub>3</sub>—was discovered independently.<sup>108</sup> Both polymorphs contain the correct trivalent lattice structure, bond geometry, and large SOC to possibly realize a Kitaev model, thereby providing a new avenue toward the discovery of a 3D spin liquid. However, magnetic orders were experimentally observed in both  $\beta$ -Li<sub>2</sub>IrO<sub>3</sub> and  $\gamma$ -Li<sub>2</sub>IrO<sub>3</sub>.<sup>109,110</sup> Similar to the two-dimensional case, both theoretical and experimental work has focused on the magnetic phases in order to understand the role played by Kitaev physics. Additionally, theoretical investigations have been undertaken to explore this new 3D spin liquid appearing in the Kitaev limit.

### 1. Experimental review

The hyper- and stripy-honeycomb iridates are built from networks of edge-shared octahedra much like the 2D honeycomb iridates, but these networks are intrinsically three-dimensional. Both of these materials are insulating, with the magnetic susceptibility indicating a moment size close to that of a spin-1/2 degree of freedom. As in the case of Na<sub>2</sub>IrO<sub>3</sub> and  $\alpha$ -Li<sub>2</sub>IrO<sub>3</sub>, this is consistent with a picture of localized  $j = 1/2$  moments. An antiferromagnetic ordering transition is seen at  $\sim 38$  K in *both* materials through a kink in the magnetic susceptibility and a peak in the specific heat, though Curie-Weiss fits demonstrate predominant ferromagnetic exchanges in both compounds.<sup>107,108</sup> In the case of  $\gamma$ -Li<sub>2</sub>IrO<sub>3</sub>, these exchanges are believed to be anisotropic as torque magnetometry measurements have revealed a temperature dependence in the anisotropy of the magnetic susceptibility.<sup>108</sup> Further studies of these orderings using magnetic resonant x-ray scattering have identified the magnetic states in both the  $\beta$ -Li<sub>2</sub>IrO<sub>3</sub> and  $\gamma$ -Li<sub>2</sub>IrO<sub>3</sub> as incommensurate, non-coplanar, counter-rotating spirals, as illustrated in Fig. 9. Particularly striking is the close agreement of the incommensurate propagation vectors  $\mathbf{Q} \sim [0.57, 0, 0]$  in both compounds.<sup>109,110</sup> While closely related, these two ordering patterns have subtle differences: In  $\beta$ -Li<sub>2</sub>IrO<sub>3</sub>, the moments projected along each of the three orthorhombic directions,  $\hat{\mathbf{a}}$ ,  $\hat{\mathbf{b}}$ , and  $\hat{\mathbf{c}}$  transform under the same irreducible representation for a magnetic structure with wave-vector  $[q, 0, 0]$ . In contrast, the  $\hat{\mathbf{a}}$  and  $\hat{\mathbf{c}}$  components of the spiral phase of  $\gamma$ -Li<sub>2</sub>IrO<sub>3</sub> transform under a different irreducible representation from that of the  $\hat{\mathbf{b}}$  component. The similarity of the orderings, ordering temperature, as well as local geometry of these crystals suggest that a common understanding might be possible.

### 2. Theory

These experimental discoveries have motivated a number of theoretical proposals to explain and explore these 3D honeycomb materials.<sup>70,111–116</sup> Several works attack  $\beta$ -Li<sub>2</sub>IrO<sub>3</sub> and  $\gamma$ -Li<sub>2</sub>IrO<sub>3</sub> directly, starting from a ferromagnetic Kitaev limit and considering the effects of further perturbations. These include the allowed nearest-neighbour exchanges discussed in Section IV A, as well as those between further neighbours and those induced by the monoclinic nature of the lattice.

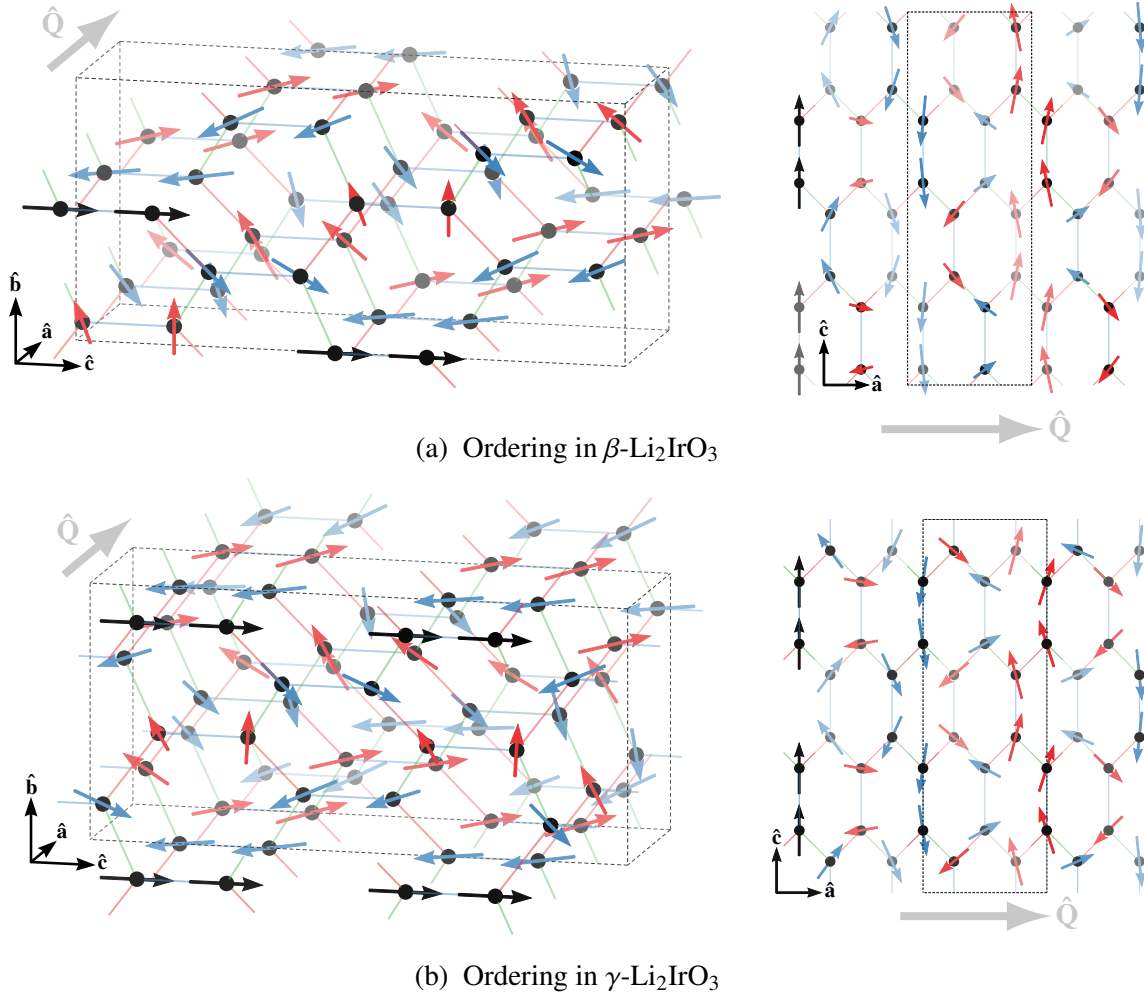


FIG. 9: Illustration of the incommensurate, non-coplanar, counter-rotating spirals in (a)  $\beta\text{-Li}_2\text{IrO}_3$ <sup>109</sup> and (b)  $\gamma\text{-Li}_2\text{IrO}_3$ <sup>110</sup>. For both these materials, the ordering wave-vector is aligned to the orthorhombic  $\hat{a}$  direction and three unit cells along that direction are depicted. The non-coplanar nature is readily seen in the perspective illustrations on the left while the counter-rotating nature of these spiral orders are evident in the projected illustration on the right. Color indicates whether the  $\hat{b}$  component of the spin is positive (red), negative (blue) or zero (black). Due to the difference in crystal symmetry of the two lattices, the  $\hat{b}$  component of the moments in  $\gamma\text{-Li}_2\text{IrO}_3$  transforms differently from the  $\hat{a}$  and  $\hat{c}$  components.

Using these interactions, several routes have been identified to stabilize an incommensurate spiral ordering near the ferromagnetic Kitaev limit<sup>70,115,116</sup>. Though capable of stabilizing the ground state, these theories have not been tested against current experimental findings such as magnetization, torque magnetometry, and thermodynamic measurements. Moreover, experiments such as inelastic scattering that probe low-energy dynamics of these systems have yet to be conducted. These comparisons and results should provide a more comprehensive understanding of the role of Kitaev physics in the unconventional magnetism encountered in these 3D honeycomb iridates.

In addition to work related to the experimental magnetic phase, theoretical work has also focused on the spin liquids that would be relevant if the Kitaev limit is stabilized on these lattices.<sup>106,111,112,117–119</sup> Identical to the 2D honeycomb case, the exact solution takes the form of free Majorana fermions in the presence of a static background  $Z_2$  gauge field, and both gapped and gapless phases can be accessed by tuning the bond anisotropy away from the isotropic limit. Unlike the 2D case, the lack of mirror symmetry implies that the background flux generated by the gauge field in the ground state may not be uniform.<sup>118</sup> Further, due to the additional constraints of the three-dimensional geometry, flux excitations of the  $Z_2$  gauge field are restricted to take the form of loops. These loops play a key role in the finite temperature properties of the model, driving a phase transition that separates the low temperature spin liquid and high temperature paramagnet<sup>117</sup>. Near the isotropic limit where the phase is gapless, the spin liquid possesses unusual nodal lines (co-dimension 2) of gapless Majorana modes. These nodal lines are topologically stable and, due to the bulk-boundary correspondence, induce gapless modes on the surface.<sup>118</sup> In the presence of time-reversal symmetry breaking, these line nodes become topologically protected Weyl points with associated surface Fermi arcs.<sup>119</sup>

Aside from the hyper- and stripy-honeycomb lattices, a number of other hypothetical trivalent lattices in three-dimensions have also been considered. The family of lattices termed the harmonic-honeycombs is a generalization of the hyper- and stripy-honeycomb lattices. These lattices are constructed by exploiting the fact that the hyper- and stripy-honeycombs can be considered as rows of honeycomb lattices stacked in an alternating fashion. By varying the number of complete honeycomb rows in such a construction, the harmonic-honeycomb series of lattices is generated. Each lattice of the series is denoted as  $\mathcal{H}\langle N \rangle$ , where  $N$  is an integer that refers to the number of complete honeycomb rows used in the construction.<sup>108</sup> The hyper- and stripy-honeycomb lattices are  $\mathcal{H}\langle 0 \rangle$  and  $\mathcal{H}\langle 1 \rangle$  respectively in this notation. Like the hyper- and stripy-honeycomb lattices, the Kitaev spin liquids in all finite- $N$  harmonic-honeycomb lattices possess topologically protected line nodes of gapless Majorana fermions and surface gapless modes.<sup>118</sup> In contrast, another 3D trivalent lattice—the hyper-octagon lattice—possesses a gapless phase with a 2D Majorana Fermi surface.<sup>120</sup> All of these theoretical lattices can be embedded in structures containing edge-shared  $\text{IrO}_6$  octahedra, hinting at the possibility of realizing a 3D Kitaev spin liquid in a yet-to-be-discovered material.

## V. OUTLOOK

The wide variety of phenomena observed and predicted in iridates and related materials has generated immense activity in the field. Our objective in this review was not to be exhaustive but rather to instill a sense of breadth by highlighting a few specific directions recent studies have pursued. In particular, we examined the Ruddlesden-Popper series of iridates and their related heterostructures where unconventional magnetism, topological band structures, and superconductivity have been seen or predicted. We also examined honeycomb materials, both in two and three

dimensions, where the joined effects of SOC, electron correlation, and lattice geometry give rise to Kitaev physics and its associated magnetism. These topics merely scratch the surface of possibilities in the study of the interplay of SOC and electronic correlations; related research directions, both theoretical and experimental, further illustrate the richness of this field. With this rapid development, however, there remain several obstacles that if resolved, can substantially enhance our understanding of SOC effects and propel the community forward.

One issue that has hindered the study of iridate materials is the large neutron absorption cross-section of Ir. This property has restricted neutron scattering experiments to powder samples or large single crystals, where the former studies lack wave-vector details while the latter studies may require years of growth technique refinement. Although great headway has been achieved using resonant X-ray scattering as an alternative probe, higher energy resolution and the ability to perturb the measured system *in situ* would enable these techniques to be a true alternative to neutron techniques. Sample quality is also in need of continual refinement in many of the considered compounds, especially the honeycomb iridates where Na and Li readily oxidizes, as discussed in Sec. IV C 1. Homogeneous solutions of single crystal of  $(\text{Na}_{1-x}\text{Li}_x)_2\text{IrO}_3$  over a wide range of  $x$  (and especially  $x = 1$ ) would greatly enhance our understanding of Kitaev physics and its connection with microscopic details of materials. In addition to elemental substitution, other methods to perturb these systems toward the Kitaev regime or MIT, for example with applied pressure, could also provide ample insight. Even with the well-studied perovskite iridates, there are still opportunities for major breakthroughs. Direct evidence of superconductivity in  $\text{Sr}_2\text{IrO}_4$  or other iridium oxides is still intensely pursued, as is evidence and examples of topological phases. Aside from strontium iridates, other avenues to realize topological phases have also been sought. As mentioned in Sec. III D, engineered phases like superlattices or thin films of  $4d$  or  $5d$  TMOs play a special role in this area of exploration due to their tunability of SOC, correlation, and lattice distortions. In this regard, materials like thin film pyrochlore iridates<sup>121–123</sup> and epitaxial perovskites<sup>39,124–126</sup> have received considerable attention. On the theoretical front, extending our understanding of topological phases of Sec. III D beyond the non-interacting limit is an important goal. A large effort has focused on the consequences of interactions and disorder in Weyl semi-metals, especially in relation to its characterization<sup>127</sup>, transport properties<sup>128,129</sup>, and instabilities towards exotic phases<sup>130–132</sup>. Related is the study of Coulomb interaction on the quadratic band touching in pyrochlore iridates, which can induce a quantum critical non-Fermi liquid, a Weyl semi-metal, or a topological insulator depending on the preserved symmetries.<sup>133</sup> These are but some examples where theoretical predictions of interacting topological phases may find realizations in iridate materials, and continual search for these systems will be a central focus in the years coming.

In addition to addressing outstanding issues, the discovery of new compounds has also driven promising lines of investigation. These new materials provide a wonderful arena both to test theoretical predictions and to discover new phenomena related to strong SOC. A recent example is the Mott-insulating  $\text{Ba}_3\text{IrTi}_2\text{O}_9$  that does not order magnetically.<sup>134</sup> It has been argued to realize the HK model on a triangular lattice, leading to frustration in both geometry *and* exchanges, which

can lead to a variety of exotic phases.<sup>2,135</sup> Another recently synthesized compound thought to host the HK model is the honeycomb  $\text{Li}_2\text{RhO}_3$ , which is closely related to the 2D honeycomb materials discussed in Sec. IV C. This  $4d^5$  material does not magnetically order but shows spin-glass behavior that may be related to disorder or stacking faults. With this reported rhodate, alluring ideas like the synthesis of 3D honeycomb rhodates or isoelectronic substitution of honeycomb materials will allow the tuning between  $4d$  and  $5d$  materials to tilt the balance between SOC, crystal field, and correlation effects.

Intimately related to lattice geometry is how the  $\text{IrO}_6$  octahedra are inter-connected; the manipulation of this connectivity has also been an interesting approach to generate new compounds. Our review has focused on corner- and edge-shared octahedra, but there are a variety of compounds with face-sharing octahedra where SOC plays an important role in the behavior of the material.<sup>136,137</sup> The Mott insulating and magnetically ordered double perovskites  $\text{La}_2\text{ZnIrO}_6$  and  $\text{La}_2\text{MgIrO}_6$  serve as yet another example<sup>138,139</sup>: the  $\text{IrO}_6$  octahedra in these double perovskites are spatially separated because they do not share corners, edges, nor faces. The resulting reduction in orbital overlaps between nearest neighbor  $5d$  Ir orbitals leads to a decrease in bandwidth or, equivalently, a relative enhancement of SOC and correlation effects. By further spatially isolating the  $\text{IrO}_6$  octahedra, the validity of the localized picture of  $j = 1/2$  orbitals can be probed. The magnetically ordered compound  $\text{Ca}_4\text{IrO}_6$  is one such example.<sup>136,140</sup> The large separation between octahedra in this compound and near-ideal  $\text{IrO}_6$  geometry has led to one of the first detections of distortion-free  $j = 1/2$  orbitals in this compound.<sup>140</sup> The compound  $\text{Sr}_x\text{La}_{11-x}\text{Ir}_4\text{O}_{24}$  has also been used to test the  $j = 1/2$  states but offers an additional twist: with the tuning of  $1 < x < 5$ , the valence of the iridium ions can be changed between  $\text{Ir}^{4+}$  ( $d^5$ ) and  $\text{Ir}^{5+}$  ( $d^4$ ).<sup>141</sup> In the strong SOC limit, the  $d^4$  filling yields a non-magnetic state since the atomic  $j = 3/2$  states are completely occupied and the  $j = 1/2$  orbitals remain unfilled. Measurements of the magnetic properties of this series of materials indeed show a transition between the  $j = 1/2$  and non-magnetic state, indicating that strong SOC is essential in the description of spatially isolated  $\text{IrO}_6$  octahedra. However, this strong SOC limit may not apply to other compounds with the  $d^4$  configuration: examples include the layered perovskite  $\text{Ca}_2\text{RuO}_4$ <sup>142</sup>, the honeycomb materials  $A_2\text{RuO}_3$  ( $A=\text{Li}, \text{Na}$ )<sup>143</sup>, and yet another variety of double perovskites,  $\text{Sr}_2\text{YIrO}_6$ <sup>144</sup> and  $\text{La}_2M\text{RuO}_6$  ( $M=\text{Mg}$  and  $\text{Zn}$ )<sup>145</sup>. Magnetic transitions have been observed in these compounds and the origin of such magnetism is under active investigation. Proposals such as Van Vleck-type Mott insulators<sup>146</sup>, strong non-cubic crystal field effects<sup>144</sup>, and competition between super-exchange and SOC<sup>147</sup> have been investigated in the context of these magnetic  $d^4$  systems.

Beyond integer fillings, systems with partial filling have also received attention and the multi-orbital nature of these transition metal compounds may play an elevated role. In the recently synthesized  $\text{Ba}_5\text{AlIr}_2\text{O}_{11}$ , dimers of face-shared  $\text{IrO}_6$  octahedra have an average valence of  $\text{Ir}^{4.5+}$ , yet the material is a Mott insulator.<sup>137</sup> In the thiospinel  $\text{CuIr}_2\text{S}_4$ , where sulphur plays the role of oxygen in the octahedral cages, the average valence is  $\text{Ir}^{3.5+}$ .<sup>148</sup> Several recent studies have shown that SOC, which have been neglected in earlier works,<sup>149</sup> may be important in the newly observed low temperature paramagnetic state.<sup>148</sup> Its cousin,  $\text{CuIr}_2\text{Se}_4$ , is a metal, but when doped with Pt,

shows evidence of superconductivity:<sup>150</sup> an exciting opportunity considering the local structural similarities between  $\text{IrSe}_6$  and the  $\text{IrO}_6$  octahedra discussed throughout this article. Another example is the hyper-kagome,  $\text{Na}_3\text{Ir}_3\text{O}_8$ , which has an average valence of  $\text{Ir}^{4.33+}$  and thus can be considered as a 1/3-doped version of the spin-liquid candidate  $\text{Na}_4\text{Ir}_3\text{O}_8$  mentioned briefly in Sec. IV D.<sup>151</sup> Unlike the Mott-insulating  $\text{Na}_4\text{Ir}_3\text{O}_8$ , this new material is semi-metallic, which was argued to stem from the presence of strong SOC and distortion-induced molecular orbitals.<sup>151</sup> With a combination of its chiral crystal structure and frustrated lattice, it was suggested that this semi-metallic material may harbour a unique platform to study non-trivial electronic transport due to topological effects arising from strong SOC.<sup>151</sup>

As we have seen in these brief examples, the study of the combined effects of strong SOC and correlations has grown to encompass a wide range of materials and phenomena. This breadth is an indication of the rapid development of this field, which boosts the prospects of discovering novel and exciting physics. With the eventual advancement in experimental, numerical, and theoretical techniques, many obstacles currently faced can be tackled, and perhaps even resolved, thus paving way for new and exciting research directions in the near future.

## ACKNOWLEDGMENTS

We thank G. K. Khaliullin, Y. J. Kim, Y. B. Kim, B. J. Kim, P. Gegenwart, J. Matsuno and R. Coldea for useful comments and discussions. This work is supported by NSERC of Canada (JR, EL, and HYK).

---

\* Electronic Address: [hykee@physics.utoronto.ca](mailto:hykee@physics.utoronto.ca)

<sup>1</sup> W. Witczak-Krempa, G. Chen, Y. B. Kim, and L. Balents, *Annual Review of Condensed Matter Physics* **5**, 57 (2014).

<sup>2</sup> G. Khaliullin, *Progress of Theoretical Physics Supplement* **160**, 155 (2005).

<sup>3</sup> A. Georges, L. de' Medici, and J. Mravlje, *Annual Review of Condensed Matter Physics* **4**, 137 (2013).

<sup>4</sup> D. van der Marel and G. A. Sawatzky, *Physical Review B* **37**, 10674 (1988).

<sup>5</sup> B. J. Kim, H. Jin, S. J. Moon, J.-Y. Kim, B.-G. Park, C. Leem, J. Yu, T. Noh, C. Kim, S.-J. Oh, J.-H. Park, V. Durairaj, G. Cao, and E. Rotenberg, *Physical Review Letters* **101**, 076402 (2008).

<sup>6</sup> M. K. Crawford, M. A. Subramanian, R. L. Harlow, J. A. Fernandez-Baca, Z. R. Wang, and D. C. Johnston, *Physical Review B* **49**, 9198 (1994).

<sup>7</sup> Q. Huang, J. Soubeyroux, O. Chmaissem, I. N. Sora, A. Santoro, R. Cava, J. Krajewski, and W. Peck, *Journal of Solid State Chemistry* **112**, 355 (1994).

<sup>8</sup> G. Cao, Y. Xin, C. Alexander, J. Crow, P. Schlottmann, M. Crawford, R. Harlow, and W. Marshall, *Physical Review B* **66**, 214412 (2002).

<sup>9</sup> J. Longo, J. Kafalas, and R. Arnott, *Journal of Solid State Chemistry* **3**, 174 (1971).



- <sup>10</sup> J. Zhao, L. Yang, Y. Yu, F. Li, R. Yu, Z. Fang, L. Chen, and C. Jin, *Journal of Applied Physics* **103**, 103706 (2008).
- <sup>11</sup> J. J. Randall Jr, L. Katz, and R. Ward, *Journal of the American Chemical Society* **79**, 266 (1957).
- <sup>12</sup> W. Komer and D. Machin, *Journal of the Less Common Metals* **61**, 91 (1978).
- <sup>13</sup> Y. Maeno, H. Hashimoto, K. Yoshida, S. Nishizaki, T. Fujita, J. Bednorz, and F. Lichtenberg, *Nature* **372**, 532 (1994).
- <sup>14</sup> G. Cao, J. Bolivar, S. McCall, J. E. Crow, and R. P. Guertin, *Physical Review B* **57**, R11039 (1998).
- <sup>15</sup> B. Kim, H. Ohsumi, T. Komesu, S. Sakai, T. Morita, H. Takagi, and T. Arima, *Science* **323**, 1329 (2009).
- <sup>16</sup> J. Kafalas and J. Longo, *Journal of Solid State Chemistry* **4**, 55 (1972).
- <sup>17</sup> S. Moon, H. Jin, K. W. Kim, W. Choi, Y. Lee, J. Yu, G. Cao, A. Sumi, H. Funakubo, C. Bernhard, and T. Noh, *Physical Review Letters* **101**, 226402 (2008).
- <sup>18</sup> I. Nagai, Y. Yoshida, S. Ikeda, H. Matsuhata, H. Kito, and M. Kosaka, *Journal of Physics: Condensed Matter* **19**, 136214 (2007).
- <sup>19</sup> J. Kim, Y. Choi, J. Kim, J. Mitchell, G. Jackeli, M. Daghofer, J. van den Brink, G. Khaliullin, and B. Kim, *Physical Review Letters* **109**, 037204 (2012).
- <sup>20</sup> S. Fujiyama, K. Ohashi, H. Ohsumi, K. Sugimoto, T. Takayama, T. Komesu, M. Takata, T. Arima, and H. Takagi, *Physical Review B* **86**, 174414 (2012).
- <sup>21</sup> F. Ye, S. Chi, B. C. Chakoumakos, J. A. Fernandez-Baca, T. Qi, and G. Cao, *Physical Review B* **87**, 140406 (2013).
- <sup>22</sup> G. Jackeli and G. Khaliullin, *Physical Review Letters* **102**, 017205 (2009).
- <sup>23</sup> J. Matsuno, K. Ihara, S. Yamamura, H. Wadati, K. Ishii, V. V. Shankar, H.-Y. Kee, and H. Takagi, *arXiv preprint arXiv:1401.1066* (2014).
- <sup>24</sup> R. Arita, J. Kuneš, A. Kozhevnikov, A. Eguiluz, and M. Imada, *Physical Review Letters* **108**, 086403 (2012).
- <sup>25</sup> D. Hsieh, F. Mahmood, D. Torchinsky, G. Cao, and N. Gedik, *Physical Review B* **86**, 035128 (2012).
- <sup>26</sup> J.-M. Carter, V. V. Shankar, and H.-Y. Kee, *Physical Review B* **88**, 035111 (2013).
- <sup>27</sup> M. Subramanian, M. Crawford, and R. Harlow, *Materials research bulletin* **29**, 645 (1994).
- <sup>28</sup> F. Wang and T. Senthil, *Physical Review Letters* **106**, 136402 (2011).
- <sup>29</sup> J. Kim, A. Said, D. Casa, M. Upton, T. Gog, M. Daghofer, G. Jackeli, J. van den Brink, G. Khaliullin, and B. Kim, *Physical Review Letters* **109**, 157402 (2012).
- <sup>30</sup> J.-M. Carter and H.-Y. Kee, *Physical Review B* **87**, 014433 (2013).
- <sup>31</sup> X.-L. Qi and S.-C. Zhang, *Reviews of Modern Physics* **83**, 1057 (2011).
- <sup>32</sup> M. Z. Hasan and J. E. Moore, *Annual Review of Condensed Matter Physics* **2**, 55 (2011).
- <sup>33</sup> A. M. Turner and A. Vishwanath, *Contemporary Concepts of Condensed Matter Science: Topological Insulators* **6**, 293 (2013).
- <sup>34</sup> A. Shitade, H. Katsura, J. Kuneš, X.-L. Qi, S.-C. Zhang, and N. Nagaosa, *Physical Review Letters* **102**, 256403 (2009).



- <sup>35</sup> I. Mazin, H. O. Jeschke, K. Foyevtsova, R. Valentí, and D. Khomskii, [Physical Review Letters](#) **109**, 197201 (2012).
- <sup>36</sup> H. Hwang, Y. Iwasa, M. Kawasaki, B. Keimer, N. Nagaosa, and Y. Tokura, [Nature materials](#) **11**, 103 (2012).
- <sup>37</sup> D. Xiao, W. Zhu, Y. Ran, N. Nagaosa, and S. Okamoto, [Nature communications](#) **2**, 596 (2011).
- <sup>38</sup> J. Lado, V. Pardo, and D. Baldomir, [Physical Review B](#) **88**, 155119 (2013).
- <sup>39</sup> S. Jang, H. Kim, S. Moon, W. Choi, B. Jeon, J. Yu, and T. Noh, [Journal of Physics: Condensed Matter](#) **22**, 485602 (2010).
- <sup>40</sup> Y. Chen and H.-Y. Kee, [Physical Review B](#) **90**, 195145 (2014).
- <sup>41</sup> L. Fu, [Physical Review Letters](#) **106**, 106802 (2011).
- <sup>42</sup> X. Wan, A. M. Turner, A. Vishwanath, and S. Y. Savrasov, [Physical Review B](#) **83**, 205101 (2011).
- <sup>43</sup> S. Matsuura, P.-Y. Chang, A. P. Schnyder, and S. Ryu, [New Journal of Physics](#) **15**, 065001 (2013).
- <sup>44</sup> Y. Chen, Y.-M. Lu, and H.-Y. Kee, [Nature communications](#) **6**, 6593 (2015).
- <sup>45</sup> J. Kim, D. Casa, M. Upton, T. Gog, Y.-J. Kim, J. Mitchell, M. Van Veenendaal, M. Daghofer, J. van den Brink, G. Khaliullin, and B. J. Kim, [Physical Review Letters](#) **108**, 177003 (2012).
- <sup>46</sup> G. Khaliullin, W. Koshibae, and S. Maekawa, [Physical Review Letters](#) **93**, 176401 (2004).
- <sup>47</sup> Z. Y. Meng, Y. B. Kim, and H.-Y. Kee, [Physical Review Letters](#) **113**, 177003 (2014).
- <sup>48</sup> P. A. Lee, N. Nagaosa, and X.-G. Wen, [Reviews of Modern Physics](#) **78**, 17 (2006).
- <sup>49</sup> O. Korneta, T. Qi, S. Chikara, S. Parkin, L. De Long, P. Schlottmann, and G. Cao, [Physical Review B](#) **82**, 115117 (2010).
- <sup>50</sup> Y. Klein and I. Terasaki, [Journal of Physics: Condensed Matter](#) **20**, 295201 (2008).
- <sup>51</sup> M. Ge, T. Qi, O. Korneta, D. De Long, P. Schlottmann, W. Crummett, and G. Cao, [Physical Review B](#) **84**, 100402 (2011).
- <sup>52</sup> Y. Kim, O. Krupin, J. Denlinger, A. Bostwick, E. Rotenberg, Q. Zhao, J. Mitchell, J. Allen, and B. Kim, [Science](#) **345**, 187 (2014).
- <sup>53</sup> Y. Cao, Q. Wang, J. A. Waugh, T. J. Reber, H. Li, X. Zhou, S. Parham, N. C. Plumb, E. Rotenberg, A. Bostwick, J. D. Denlinger, T. Qi, M. A. Hermele, G. Cao, and D. S. Dessau, [arXiv preprint arXiv:1406.4978](#) (2014).
- <sup>54</sup> L. Li, P. Kong, T. Qi, C. Jin, S. Yuan, L. DeLong, P. Schlottmann, and G. Cao, [Physical Review B](#) **87**, 235127 (2013).
- <sup>55</sup> Y. Liu, L. Yu, X. Jia, J. Zhao, H. Weng, Y. Peng, C. Chen, Z. Xie, D. Mou, J. He, X. Liu, Y. Feng, H. Yi, L. Zho, G. Liu, S. He, X. Dong, J. Zhang, Z. Xu, C. Chen, G. Cao, X. Dai, Z. Fang, and X. J. Zhou, [arXiv preprint arXiv:1501.04687](#) (2015).
- <sup>56</sup> J. He, H. Hafiz, T. R. Mion, T. Hogan, C. Dhital, X. Chen, Q. Lin, M. Hashimoto, D. Lu, Y. Zhang, R. S. Markiewicz, A. Bansil, S. D. Wilson, and R.-H. He, [Scientific reports](#) **5**, 8533 (2015).
- <sup>57</sup> A. Kitaev, [Annals of Physics](#) **321**, 2 (2006).
- <sup>58</sup> Z. Nussinov and J. van den Brink, [Reviews of Modern Physics](#) **87**, 1 (2015).
- <sup>59</sup> Imposing the local plaquette symmetries of the Kitaev model *does* achieve this, but these are not present

in the microscopic physics.

- <sup>60</sup> J. Chaloupka, G. Jackeli, and G. Khaliullin, [Physical Review Letters](#) **105**, 027204 (2010).
- <sup>61</sup> J. Chaloupka, G. Jackeli, and G. Khaliullin, [Physical Review Letters](#) **110**, 097204 (2013).
- <sup>62</sup> J. G. Rau, E. K.-H. Lee, and H.-Y. Kee, [Physical Review Letters](#) **112**, 077204 (2014).
- <sup>63</sup> J. G. Rau and H.-Y. Kee, [arXiv preprint arXiv:1408.4811](#) (2014).
- <sup>64</sup> I. Kimchi and Y.-Z. You, [Physical Review B](#) **84**, 180407 (2011).
- <sup>65</sup> V. M. Katukuri, S. Nishimoto, V. Yushankhai, A. Stoyanova, H. Kandpal, S. Choi, R. Coldea, I. Rousochatzakis, L. Hozoi, and J. van den Brink, [New Journal of Physics](#) **16**, 013056 (2014).
- <sup>66</sup> Y. Yamaji, Y. Nomura, M. Kurita, R. Arita, and M. Imada, [Physical Review Letters](#) **113**, 107201 (2014).
- <sup>67</sup> Y. Sizyuk, C. Price, P. Wölfle, and N. B. Perkins, [Physical Review B](#) **90**, 155126 (2014).
- <sup>68</sup> R. Comin, G. Levy, B. Ludbrook, Z.-H. Zhu, C. Veenstra, J. Rosen, Y. Singh, P. Gegenwart, D. Stricker, J. N. Hancock, D. van der Marel, I. S. Elfimov, and A. Damascelli, [Physical Review Letters](#) **109**, 266406 (2012).
- <sup>69</sup> S. Lee, J.-S. Jeong, K. Hwang, and Y. B. Kim, [Physical Review B](#) **90**, 134425 (2014).
- <sup>70</sup> I. Kimchi, R. Coldea, and A. Vishwanath, [arXiv preprint arXiv:1408.3640](#) (2014).
- <sup>71</sup> Y. Singh and P. Gegenwart, [Physical Review B](#) **82**, 064412 (2010).
- <sup>72</sup> Y. Singh, S. Manni, J. Reuther, T. Berlijn, R. Thomale, W. Ku, S. Trebst, and P. Gegenwart, [Physical Review Letters](#) **108**, 127203 (2012).
- <sup>73</sup> F. Ye, S. Chi, H. Cao, B. C. Chakoumakos, J. A. Fernandez-Baca, R. Custelcean, T. Qi, O. Korneta, and G. Cao, [Physical Review B](#) **85**, 180403 (2012).
- <sup>74</sup> S. Choi, R. Coldea, A. Kolmogorov, T. Lancaster, I. Mazin, S. Blundell, P. Radaelli, Y. Singh, P. Gegenwart, K. Choi, S.-W. Cheong, P. J. Baker, C. Stock, and J. Taylor, [Physical Review Letters](#) **108**, 127204 (2012).
- <sup>75</sup> H. Gretarsson, J. P. Clancy, X. Liu, J. P. Hill, E. Bozin, Y. Singh, S. Manni, P. Gegenwart, J. Kim, A. H. Said, D. Casa, T. Gog, M. H. Upton, H.-S. Kim, J. Yu, V. M. Katukuri, L. Hozoi, J. van den Brink, and Y.-J. Kim, [Physical Review Letters](#) **110**, 076402 (2013).
- <sup>76</sup> X. Liu, T. Berlijn, W.-G. Yin, W. Ku, A. Tsvelik, Y.-J. Kim, H. Gretarsson, Y. Singh, P. Gegenwart, and J. Hill, [Physical Review B](#) **83**, 220403 (2011).
- <sup>77</sup> H. Gretarsson, J. Clancy, Y. Singh, P. Gegenwart, J. Hill, J. Kim, M. Upton, A. Said, D. Casa, T. Gog, and Y.-J. Kim, [Physical Review B](#) **87**, 220407 (2013).
- <sup>78</sup> S. H. Chun, J.-W. Kim, J. Kim, H. Zheng, C. C. Stoumpos, C. Malliakas, J. Mitchell, K. Mehlawat, Y. Singh, Y. Choi, T. Gog, A. Al-Zein, M. Moretti Sala, M. Krisch, J. Chaloupka, G. Jackeli, G. Khaliullin, and B. J. Kim, [Nature Physics](#) (2015), 10.1038/nphys3322.
- <sup>79</sup> R. Coldea, Talk at the SPORE13 conference held at MPIPKS, Dresden (2013); S. Choi, Talk at the APS March meeting, Denver, CO (2014).
- <sup>80</sup> G. Cao, T. F. Qi, L. Li, J. Terzic, V. S. Cao, S. J. Yuan, M. Tovar, G. Murthy, and R. K. Kaul, [Physical Review B](#) **88**, 220414 (2013).
- <sup>81</sup> S. Manni, S. Choi, I. Mazin, R. Coldea, M. Altmeyer, H. O. Jeschke, R. Valenti, and P. Gegenwart,

- [Physical Review B \*\*89\*\*, 245113 \(2014\).](#)
- <sup>82</sup> S. Manni, Y. Tokiwa, and P. Gegenwart, [Physical Review B \*\*89\*\*, 241102 \(2014\).](#)
- <sup>83</sup> H.-C. Jiang, Z.-C. Gu, X.-L. Qi, and S. Trebst, [Physical Review B \*\*83\*\*, 245104 \(2011\).](#)
- <sup>84</sup> J. Reuther, R. Thomale, and S. Trebst, [Physical Review B \*\*84\*\*, 100406 \(2011\).](#)
- <sup>85</sup> C. C. Price and N. B. Perkins, [Physical Review Letters \*\*109\*\*, 187201 \(2012\).](#)
- <sup>86</sup> Y.-Z. You, I. Kimchi, and A. Vishwanath, [Physical Review B \*\*86\*\*, 085145 \(2012\).](#)
- <sup>87</sup> R. Schaffer, S. Bhattacharjee, and Y. B. Kim, [Physical Review B \*\*86\*\*, 224417 \(2012\).](#)
- <sup>88</sup> J. Chaloupka and G. Khaliullin, [arXiv preprint arXiv:1502.02587 \(2015\).](#)
- <sup>89</sup> S. Nishimoto, V. M. Katukuri, V. Yushankhai, H. Stoll, U. K. Roessler, L. Hozoi, I. Rousochatzakis, and J. van den Brink, [arXiv preprint arXiv:1403.6698 \(2014\).](#)
- <sup>90</sup> E. Stroganov and K. Ovchinnikov, *Vestnik. Leningrad. Univ., Ser. Fiz. i Khim.* **12**, 152.
- <sup>91</sup> L. Binotto, I. Pollini, and G. Spinolo, [physica status solidi \(b\) \*\*44\*\*, 245 \(1971\).](#)
- <sup>92</sup> I. Pollini, [Physical Review B \*\*53\*\*, 12769 \(1996\).](#)
- <sup>93</sup> K. Plumb, J. Clancy, L. Sandilands, V. V. Shankar, Y. Hu, K. Burch, H.-Y. Kee, and Y.-J. Kim, [Physical Review B \*\*90\*\*, 041112 \(2014\).](#)
- <sup>94</sup> J. Fletcher, W. Gardner, A. Fox, and G. Topping, [Journal of the Chemical Society A: Inorganic, Physical, Theoretical , 1038 \(1967\).](#)
- <sup>95</sup> Y. Kobayashi, T. Okada, K. Asai, M. Katada, H. Sano, and F. Ambe, [Inorganic Chemistry \*\*31\*\*, 4570 \(1992\).](#)
- <sup>96</sup> Y. Kubota, H. Tanaka, T. Ono, Y. Narumi, and K. Kindo, [Physical Review B \*\*91\*\*, 094422 \(2015\).](#)
- <sup>97</sup> J. A. Sears, M. Songvilay, K. W. Plumb, J. P. Clancy, Y. Qiu, Y. Zhao, D. Parshall, and Y.-J. Kim, [Physical Review B \*\*91\*\*, 144420 \(2015\).](#)
- <sup>98</sup> M. Majumder, M. Schmidt, H. Rosner, A. A. Tsirlin, H. Yasuoka, and M. Baenitz, [Physical Review B \*\*91\*\*, 180401 \(2015\).](#)
- <sup>99</sup> A. Banerjee, C. Bridges, J. Yan, A. Aczel, L. Li, M. Stone, G. Granroth, M. Lumsden, Y. Yiu, J. Knolle, D. Kovrizhin, S. Bhattacharjee, R. Moessner, D. Tennant, D. Mandrus, and S. E. Nagler, [arXiv preprint arXiv:1504.08037 \(2015\).](#)
- <sup>100</sup> L. J. Sandilands, Y. Tian, A. A. Reijnders, H.-S. Kim, K. W. Plumb, H.-Y. Kee, Y.-J. Kim, and K. S. Burch, [arXiv preprint arXiv:1503.07593 \(2015\).](#)
- <sup>101</sup> V. V. Shankar, H.-S. Kim, and H.-Y. Kee, [arXiv preprint arXiv:1411.6623 \(2014\).](#)
- <sup>102</sup> B. Canals and C. Lacroix, [Physical Review Letters \*\*80\*\*, 2933 \(1998\).](#)
- <sup>103</sup> M. J. Gingras and P. A. McClarty, [Reports on Progress in Physics \*\*77\*\*, 056501 \(2014\).](#)
- <sup>104</sup> Y. Okamoto, M. Nohara, H. Aruga-Katori, and H. Takagi, [Physical Review Letters \*\*99\*\*, 137207 \(2007\).](#)
- <sup>105</sup> Y. Singh, Y. Tokiwa, J. Dong, and P. Gegenwart, [Physical Review B \*\*88\*\*, 220413 \(2013\).](#)
- <sup>106</sup> S. Mandal and N. Surendran, [Physical Review B \*\*79\*\*, 024426 \(2009\).](#)
- <sup>107</sup> T. Takayama, A. Kato, R. Dinnebier, J. Nuss, H. Kono, L. S. I. Veiga, G. Fabbri, D. Haskel, and H. Takagi, [Physical Review Letters \*\*114\*\*, 077202 \(2015\).](#)
- <sup>108</sup> K. Modic, T. E. Smidt, I. Kimchi, N. P. Breznay, A. Biffin, S. Choi, R. D. Johnson, R. Coldea,

- P. Watkins-Curry, G. T. McCandless, J. Y. Chan, F. Gandara, Z. Islam, A. Vishwanath, A. Shekhter, R. D. McDonald, and J. G. Analytis, [Nature communications](#) **5**, 4203 (2014).
- <sup>109</sup> A. Biffin, R. Johnson, S. Choi, F. Freund, S. Manni, A. Bombardi, P. Manuel, P. Gegenwart, and R. Coldea, [Physical Review B](#) **90**, 205116 (2014).
- <sup>110</sup> A. Biffin, R. Johnson, I. Kimchi, R. Morris, A. Bombardi, J. Analytis, A. Vishwanath, and R. Coldea, [Physical Review Letters](#) **113**, 197201 (2014).
- <sup>111</sup> E. K.-H. Lee, R. Schaffer, S. Bhattacharjee, and Y. B. Kim, [Physical Review B](#) **89**, 045117 (2014).
- <sup>112</sup> I. Kimchi, J. G. Analytis, and A. Vishwanath, [Physical Review B](#) **90**, 205126 (2014).
- <sup>113</sup> E. K.-H. Lee, S. Bhattacharjee, K. Hwang, H.-S. Kim, H. Jin, and Y. B. Kim, [Physical Review B](#) **89**, 205132 (2014).
- <sup>114</sup> S. Lee, E. K.-H. Lee, A. Paramakanti, and Y. B. Kim, [Physical Review B](#) **89**, 014424 (2014).
- <sup>115</sup> E. K.-H. Lee and Y. B. Kim, [Physical Review B](#) **91**, 064407 (2015).
- <sup>116</sup> H.-S. Kim, E. K.-H. Lee, and Y. B. Kim, [arXiv preprint arXiv:1502.00006](#) (2015).
- <sup>117</sup> J. Nasu, M. Udagawa, and Y. Motome, [Physical Review Letters](#) **113**, 197205 (2014).
- <sup>118</sup> R. Schaffer, E. K.-H. Lee, Y.-M. Lu, and Y. B. Kim, [Physical Review Letters](#) **114**, 116803 (2015).
- <sup>119</sup> M. Hermanns, K. O'Brien, and S. Trebst, [Physical Review Letters](#) **114**, 157202 (2015).
- <sup>120</sup> M. Hermanns and S. Trebst, [Physical Review B](#) **89**, 235102 (2014).
- <sup>121</sup> X. Hu, A. Rüegg, and G. A. Fiete, [Physical Review B](#) **86**, 235141 (2012).
- <sup>122</sup> B.-J. Yang and N. Nagaosa, [Physical Review Letters](#) **112**, 246402 (2014).
- <sup>123</sup> E. Bergholtz, Z. Liu, M. Trescher, R. Moessner, and M. Udagawa, [Physical Review Letters](#) **114**, 016806 (2015).
- <sup>124</sup> J. Nichols, J. Terzic, E. Bittle, O. Korneta, L. De Long, J. Brill, G. Cao, and S. Seo, [Applied Physics Letters](#) **102**, 141908 (2013).
- <sup>125</sup> D. Hirai, J. Matsuno, and H. Takagi, [arXiv preprint arXiv:1501.01433](#) (2015).
- <sup>126</sup> A. Biswas and Y. H. Jeong, [Journal of Applied Physics](#) **117**, 195305 (2015).
- <sup>127</sup> W. Witczak-Krempa, M. Knap, and D. Abanin, [Physical Review Letters](#) **113**, 136402 (2014).
- <sup>128</sup> A. Burkov, M. Hook, and L. Balents, [Physical Review B](#) **84**, 235126 (2011).
- <sup>129</sup> P. Hosur, S. Parameswaran, and A. Vishwanath, [Physical Review Letters](#) **108**, 046602 (2012).
- <sup>130</sup> Z. Wang and S.-C. Zhang, [Physical Review B](#) **87**, 161107 (2013).
- <sup>131</sup> J. Maciejko and R. Nandkishore, [Physical Review B](#) **90**, 035126 (2014).
- <sup>132</sup> A. Sekine and K. Nomura, [Journal of the Physical Society of Japan](#) **83**, 094710 (2014).
- <sup>133</sup> E.-G. Moon, C. Xu, Y. B. Kim, and L. Balents, [Physical Review Letters](#) **111**, 206401 (2013).
- <sup>134</sup> T. Dey, A. Mahajan, P. Khuntia, M. Baenitz, B. Koteswararao, and F. Chou, [Physical Review B](#) **86**, 140405 (2012).
- <sup>135</sup> M. Becker, M. Hermanns, B. Bauer, M. Garst, and S. Trebst, [Physical Review B](#) **91**, 155135 (2015).
- <sup>136</sup> G. Cao, V. Durairaj, S. Chikara, S. Parkin, and P. Schlottmann, [Physical Review B](#) **75**, 134402 (2007).
- <sup>137</sup> J. Terzic, J. Wang, F. Ye, W. Song, S. Yuan, S. Aswartham, L. DeLong, S. Streltsov, D. Khomskii, and G. Cao, [arXiv preprint arXiv:1505.01436](#) (2015).

- <sup>138</sup> G. Cao, A. Subedi, S. Calder, J.-Q. Yan, J. Yi, Z. Gai, L. Poudel, D. J. Singh, M. D. Lumsden, A. D. Christianson, B. C. Sales, and D. Mandrus, [Physical Review B \*\*87\*\*, 155136 \(2013\)](#).
- <sup>139</sup> A. M. Cook, S. Matern, C. Hickey, A. A. Aczel, and A. Paramakanti, [arXiv preprint arXiv:1502.01031 \(2015\)](#).
- <sup>140</sup> S. Calder, G.-X. Cao, S. Okamoto, J.-W. Kim, V. R. Cooper, Z. Gai, B. C. Sales, M. D. Lumsden, D. Mandrus, and A. D. Christianson, [Physical Review B \*\*89\*\*, 081104 \(2014\)](#).
- <sup>141</sup> B. F. Phelan, J. Krizan, W. Xie, Q. Gibson, and R. Cava, [Physical Review B \*\*91\*\*, 155117 \(2015\)](#).
- <sup>142</sup> T. Mizokawa, L. Tjeng, G. Sawatzky, G. Ghiringhelli, O. Tjernberg, N. Brookes, H. Fukazawa, S. Nakatsuji, and Y. Maeno, [Physical Review Letters \*\*87\*\*, 077202 \(2001\)](#).
- <sup>143</sup> J. Wang, J. Terzic, T. Qi, F. Ye, S. Yuan, S. Aswartham, S. Streltsov, D. Khomskii, R. Kaul, and G. Cao, [Physical Review B \*\*90\*\*, 161110 \(2014\)](#).
- <sup>144</sup> G. Cao, T. Qi, L. Li, J. Terzic, S. Yuan, L. E. DeLong, G. Murthy, and R. K. Kaul, [Physical Review Letters \*\*112\*\*, 056402 \(2014\)](#).
- <sup>145</sup> R. Dass, J.-Q. Yan, and J. Goodenough, [Physical Review B \*\*69\*\*, 094416 \(2004\)](#).
- <sup>146</sup> G. Khaliullin, [Physical Review Letters \*\*111\*\*, 197201 \(2013\)](#).
- <sup>147</sup> O. N. Meetei, W. S. Cole, M. Randeria, and N. Trivedi, [Physical Review B \*\*91\*\*, 054412 \(2015\)](#).
- <sup>148</sup> K. Kojima, R. Kadono, M. Miyazaki, M. Hiraishi, I. Yamauchi, A. Koda, Y. Tsuchiya, H. Suzuki, and H. Kitazawa, [Physical Review Letters \*\*112\*\*, 087203 \(2014\)](#).
- <sup>149</sup> D. Khomskii and T. Mizokawa, [Physical Review Letters \*\*94\*\*, 156402 \(2005\)](#).
- <sup>150</sup> H. Luo, T. Klimczuk, L. Muehler, L. Schoop, D. Hirai, M. Fuccillo, C. Felser, and R. Cava, [Physical Review B \*\*87\*\*, 214510 \(2013\)](#).
- <sup>151</sup> T. Takayama, A. Yaresko, A. Matsumoto, J. Nuss, K. Ishii, M. Yoshida, J. Mizuki, and H. Takagi, [Scientific reports \*\*4\*\*, 6818 \(2014\)](#).